The Control of a Mobile Robot with Dual Wheel Transmission

TR-CIM-10-25   October 2012

Master of Engineering Project Report

Yann Goulet Garneau

Supervisors: Jorge Angeles and Alessio Salerno

Department of Mechanical Engineering &
Centre for Intelligent Machines,
McGill University, Montreal, Canada

Abstract

This report describes the kinematics, dynamics, control and mechatronics implementation of a mobile robot with dual wheel transmission. The robot comprises four wheels, two of which are coupled to two motors via a transmission which can pivot about the steering axis. The prototype structure is made of LEGO parts and custom stainless steel axles. The kinematics of the robot is described in terms of the twist of the 12 moving assemblies of the robot. Inertial and mass parameters of the moving assemblies are evaluated using a 3D CAD model in SolidWorks. The equations of motion of the system are derived in terms of the acceleration of the two actuated wheels and a configuration parameter of the robot in Maple. The state-space form of the system is used along with pole placement to define a controller for the configuration-dependent robot model. Simulation runs under Simulink are performed to validate the controller. The mechatronics implementation is done using the Arduino platform. Finally, recommendations for future work are proposed.

1 Introduction

Wheeled mobile robots (WMR) are increasingly used in the manufacturing and distribution industry. The dual wheel transmission (DWT) is a design that aims to increase the mobility and manoeuvrability of WMR in constrained environments. The DWT couples two motors with corresponding wheels via a composite gear train which can pivot about the steering axis. Two epicyclic gear trains are used to transfer the motion of each motor to its corresponding wheel. The DWT was patented in 2005 by Angeles [1]. A sketch of the original DWT design is shown in Fig. 1a.

(a)   (b)
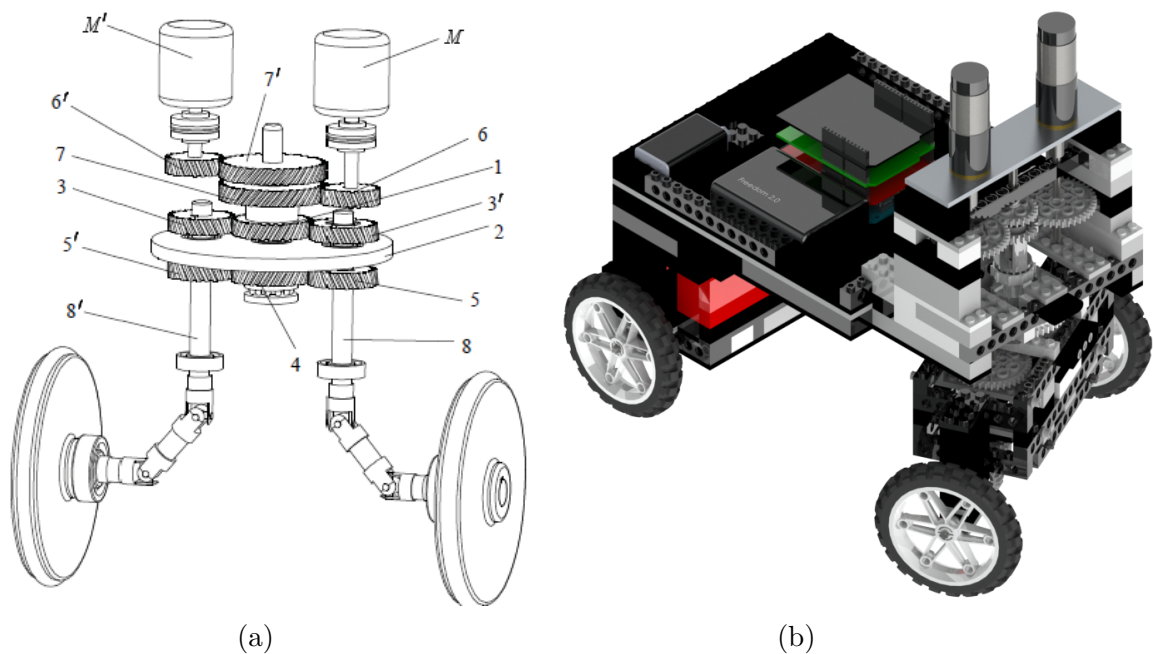
Figure 1: (a) The original DWT design sketch   (b) The robot prototype

The symmetric design of the DWT allows equal loading on both motors, uniform wear of gears and tires, unlimited rotation of the actuated-wheel axis around the steering axis and eliminates wire entanglement that would occur with the motors connected directly to the wheels.

The robot described in this report carries two identical motors mounted onto a chassis with one DWT. The robot motion can be associated with that of an articulated vehicle or a two-wheel robot with a trailer. The robot prototype is made of standard LEGO parts with

custom stainless steel shafts. A 3D model of the robot was developed with SolidWorks. It is shown in Fig. 1b. In order to stiffen the original design, bevel gears were used on the LEGO prototype instead of universal joints.

This project is part of ongoing R&D effort; it follows preliminary work by Husseini [2], Pavlov [3] and Mak [4]. The objectives of this project are to develop the robot kinematics and dynamic models, define a suitable control algorithm and implement it on the robot prototype.

The report includes sections on the mathematical modelling, control and mechatronics implementation of the robot, followed with conclusions and recommendations for future research. In the mathematical modelling section, a description of the structure of the robot and its 12 moving rigid assemblies is first included. The kinematics equations of the robot are then derived, followed by a description of the method used to derive the dynamics equations of the system. In the control section, the dynamics equations are transformed into state-space form, linearized, and then used along with pole placement to find a suitable feedback control for the robot. Finally, the mechatronics implementation section gives a description of the different components used to drive the system and control its behaviour.

2   Mathematical Modeling

We set out to define a control algorithm for the robot based on the dynamics of the system. The derivation of the mathematical model describing the kinematics and dynamics of the system is based on the study of robotic mechanical systems and rolling robots by Angeles [5].

Our approach will be one of multi-body dynamics; for this reason, we distinguish 12 rigid-body assemblies composing the robotic mechanical system. The moving assemblies are shown in Fig. 2.

We label the rigid body assemblies with numbers as indicated below:

1. Front left wheel assembly
2. Front right wheel assembly
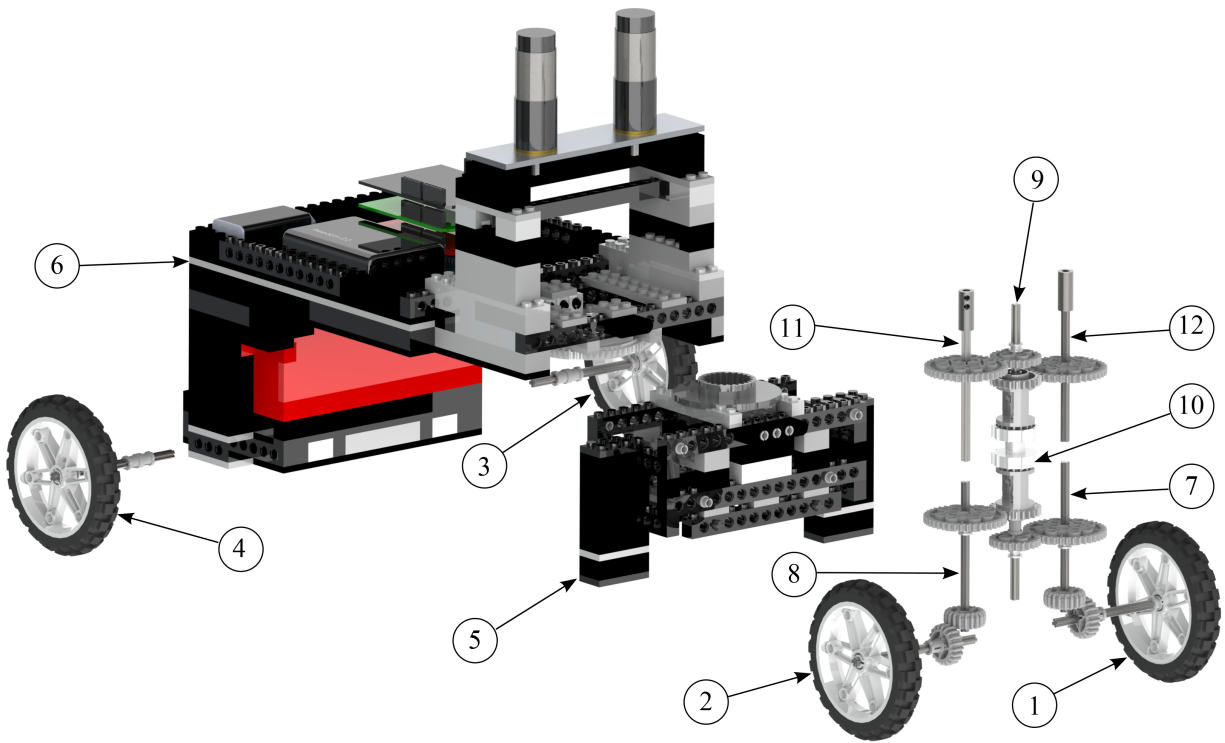3. Rear left wheel assembly
4. Rear right wheel assembly
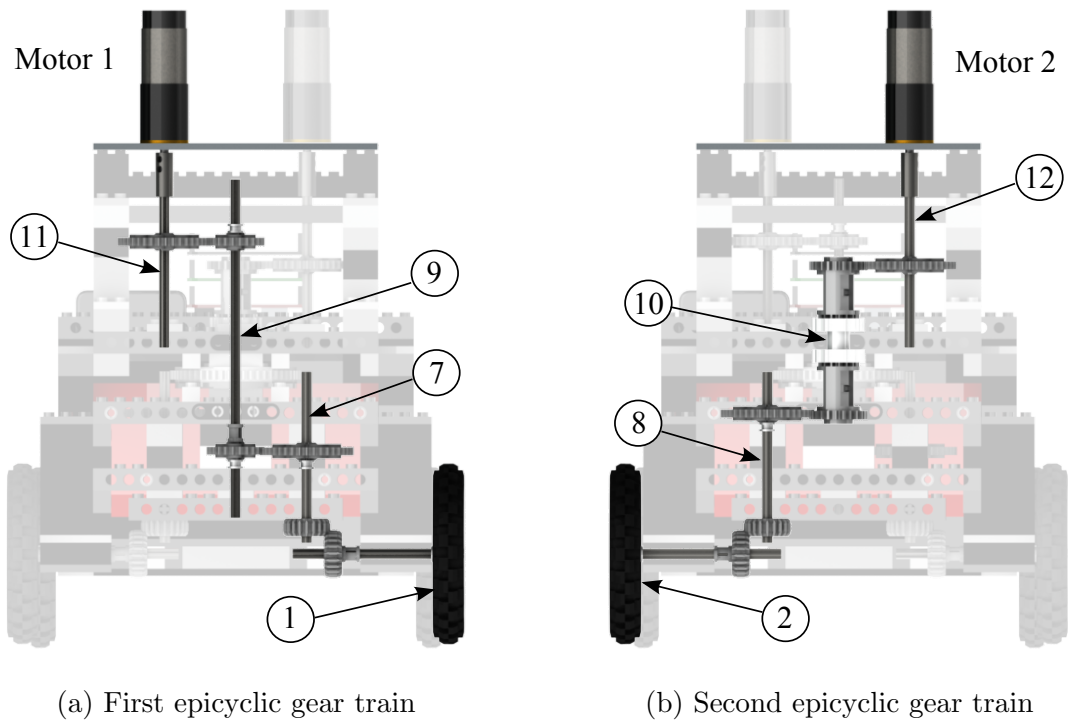
Figure 2: The 12 moving assemblies of the robot

(a) First epicyclic gear train

(b) Second epicyclic gear train

Figure 3: The transmission of the robot

5. Planet-carrier	9. Inner sun gear assembly
6. Chassis	10. Outer sun gear assembly
7. Lower left gear assembly	11. Upper right gear assembly
8. Lower right gear assembly	12. Upper left gear assembly.

The DWT comprises two epicyclic gear mechanisms coupled by the planet-carrier. The first epicyclic gear train consists of parts 1, 7, 9 and 11 and is connected to motor 1 as shown in Fig. 3a. The second epicyclic gear train consists of parts 2, 8, 10 and 12 and is connected to motor 2 as shown in Fig. 3b.

2.1   Kinematics

In deriving the mathematical model, we assume that the robot, except for its wheels, undergoes planar motion on a horizontal surface. All the rigid assemblies except the robot's four wheel assemblies undergo planar motion. We also assume that the wheels are always in contact with the ground, without slipping or slidding, and that internal dissipation such as dry and viscous friction is negligible [6].

The basic variables required to describe the kinematics of the robot are shown in Fig. 4. Let $\{O, X, Y, Z\}$ be the inertial frame $\mathcal{F}$ attached to the ground, with the Z-axis vertical and with point O attached to the ground surface.

We define θ_1 and θ_2 as the angular displacements of the two front wheels, which are actuated. It is assumed that having both $\dot{\theta}_1$ and $\dot{\theta}_2$ positive makes the planet-carrier, and hence, the axles of the wheels go forward, as indicated with $\mathbf{v}_5$ in Fig. 4. We also define $\dot{\phi}_1$ and $\dot{\phi}_2$ as the angular speeds of motors 1 and 2, which are provided with encoders to measure there speeds. It is important to note that the angular speed of the motors and the angular speed of the wheels are not simply related to the gear ratios of the two epicyclic gear trains. Indeed, the upper left and right gear assemblies (11, 12) rotate around the inner and outer sun gear assemblies (9, 10). The equations relating the angular speed of the two actuated wheels to the angular speed of the motors are derived later in the report.
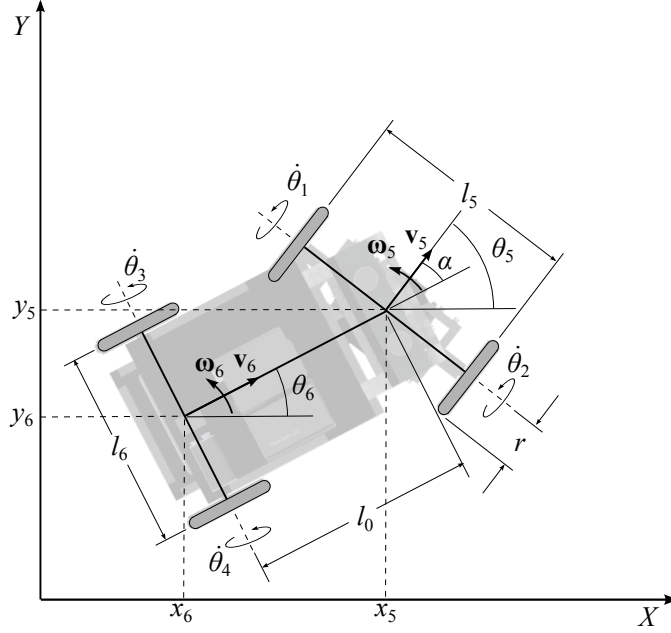
6

Figure 4: Sketch for the kinematics of the robot

We also define the actuated joint variables grouped into vector $\boldsymbol{\theta}_a$, with their time-derivatives being the actuated joint rates, grouped into vector, $\dot{\boldsymbol{\theta}}_a$, as:

$$\boldsymbol{\theta}_a \equiv \begin{bmatrix} \theta_1 & \theta_2 \end{bmatrix}^T, \quad \dot{\boldsymbol{\theta}}_a \equiv \begin{bmatrix} \dot{\theta}_1 & \dot{\theta}_2 \end{bmatrix}^T. \tag{1}$$

For the derivation of the kinematic equations of the robot, the methodology of the Natural Orthogonal Compliment (NOC) is used [5]. The methodology exploits our ability to express the kinematic constraints on the robot as a linear homogenous system of equations in the vector array of body twists. The twist of the ith rigid body $\mathbf{t}_i$ is given by:

$$\mathbf{t}_i \equiv \begin{bmatrix} \mathbf{v}_i \\ \boldsymbol{\omega}_i \end{bmatrix}, \tag{2}$$

where $\mathbf{v}_i$ is the absolute velocity vector of frame $\mathcal{F}_i$, attached to the ith rigid body, and $\boldsymbol{\omega}_i$ is the absolute angular velocity vector of the ith body expressed in the inertial reference frame.

Given the nonholonomy of the system at hand, we cannot obtain $\mathbf{v}_i$ and $\boldsymbol{\omega}_i$ in terms of only $\boldsymbol{\theta}_a$. We need a third variable to define the twist $\mathbf{t}_i$ of the robot. We use angle α, defined

7

as that between the midplane of the the two front wheels and the midplane of the two rear wheels, as per Fig. 4, i.e.,

$$\alpha = \theta_5 - \theta_6. \tag{3}$$

Next, the twists $\mathbf{t}_i$ are expressed as linear transformations of $\dot{\boldsymbol{\theta}}_a$:

$$\mathbf{t}_i = \mathbf{T}_i(\alpha)\dot{\boldsymbol{\theta}}_a, \tag{4}$$

where $\mathbf{T}_i(\alpha)$ is the 6×2 *twist-shaping matrix* of the ith rigid body, which is the *NOC* of the matrix $\mathbf{K}$ of kinematic constraints [5], that need not be explicitly calculated in this analysis.

Note here that only the twists of the chassis, upper left gear, upper right gear, rear left wheel and rear right wheel assemblies (3, 4, 6, 11, 12) are dependent on both angle α and $\dot{\boldsymbol{\theta}}_a$. The twists of the planet-carrier, left wheel, right wheel, lower left gear, lower right gear, inner sun gear, outer sun gear assemblies (1, 2, 5, 7, 8, 9, 10) can be expressed as functions of $\dot{\boldsymbol{\theta}}_a$ alone.

We now derive the absolute velocity $\mathbf{v}_i$ and absolute angular velocity $\boldsymbol{\omega}_i$ for each rigid body as a function of α, $\dot{\theta}_1$ and $\dot{\theta}_2$. Combining those two vectors yields the twist $\mathbf{t}_i$ of the ith rigid body which can then be used to find the twist shaping matrices $\mathbf{T}_i(\alpha)$ of the same rigid body. This task was achieved with the aid of Maple.

Planet-carrier (5)

The variables describing the kinematics of the planet-carrier are shown in Fig. 5. Let $\{O_5, X_5, Y_5, Z_5\}$ be the frame $\mathcal{F}_5$ attached to the planet-carrier, with O_5 located at the intersection of the midplane of the two front wheels and the axis of rotation of the same wheels. Furthermore, let $\mathbf{Q}_5$ be the 3×3 orthogonal matrix that rotates frame $\mathcal{F}_5$ with respect to the inertial frame $\mathcal{F}$ attached to the ground around the Z axis through an angle θ_5:

$$\mathbf{Q}_5 = \begin{bmatrix} \cos\theta_5 & -\sin\theta_5 & 0 \\ \sin\theta_5 & \cos\theta_5 & 0 \\ 0 & 0 & 1 \end{bmatrix}. \tag{5}$$
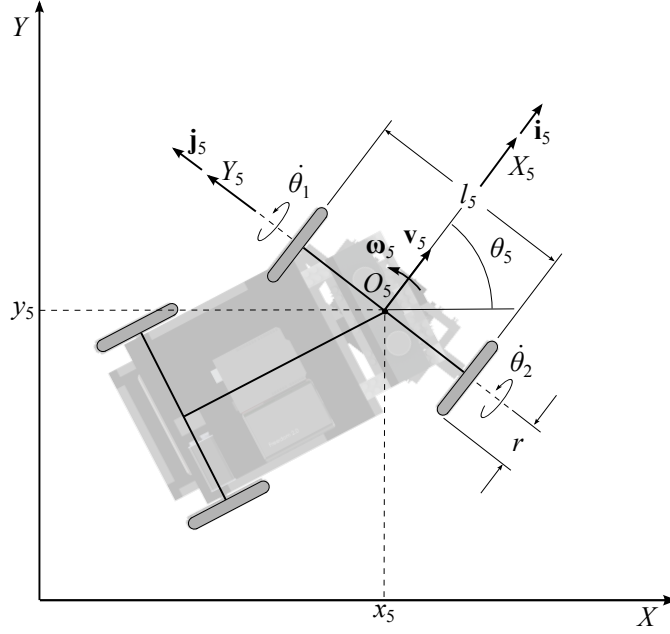
Figure 5: Sketch for the kinematics of the planet-carrier

The position vector $\mathbf{o}_5$ of the origin O_5 of the frame $\mathcal{F}_5$ is given by:

$$\mathbf{o}_5 = x_5\mathbf{i} + y_5\mathbf{j} + r\mathbf{k}. \tag{6}$$

The absolute velocity $\mathbf{v}_5$ and absolute angular velocity $\boldsymbol{\omega}_5$ of the planet-carrier, expressed in frame $\mathcal{F}_5$, are given by:

$$\mathbf{v}_5 = \frac{r}{2}(\dot{\theta}_1 + \dot{\theta}_2)\,\mathbf{i}_5, \tag{7}$$

$$\boldsymbol{\omega}_5 = \frac{r}{l_5}(\dot{\theta}_2 - \dot{\theta}_1)\,\mathbf{k}_5. \tag{8}$$

The position vector of the planet-carrier, $[x_5\ y_5\ \theta_5]^T$, can be derived from the relations

$$\dot{\theta}_5 = \omega_5, \quad \dot{x}_5 = v_5\cos\theta_5, \quad \dot{y}_5 = v_5\sin\theta_5. \tag{9}$$

9

Chassis (6)

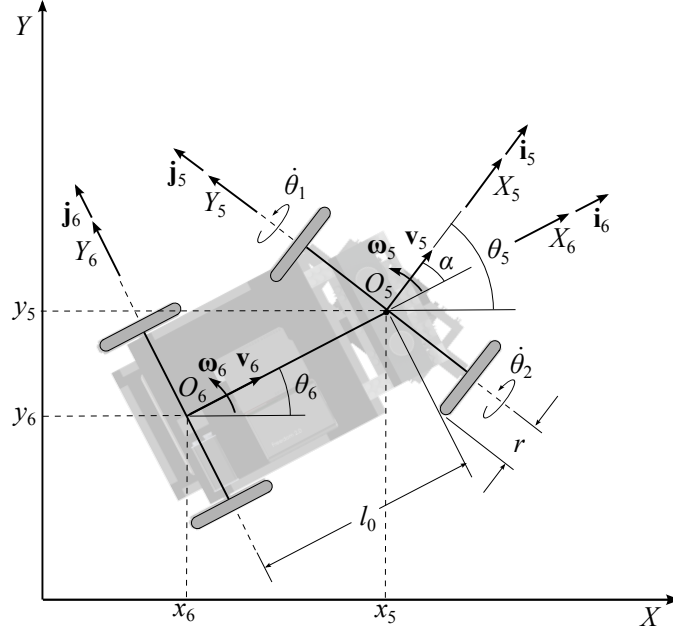The variables describing the kinematics of the chassis are shown in Fig. 6.

Figure 6: Sketch for the kinematics of the chassis

Let $\{O_6, X_6, Y_6, Z_6\}$ be the frame $\mathcal{F}_6$ attached to the planet-carrier, with origin O_6 located at the intersection of the midplane of the two rear wheels and the axis of rotation of the two same wheels.

Furthermore, let $\mathbf{Q}_6$ be the 3×3 orthogonal matrix that rotates frame $\mathcal{F}_6$ with respect to the frame $\mathcal{F}_5$ around the Z_5 axis through an angle α:

$$\mathbf{Q}_6 = \begin{bmatrix} \cos\alpha & \sin\alpha & 0 \\ -\sin\alpha & \cos\alpha & 0 \\ 0 & 0 & 1 \end{bmatrix}. \tag{10}$$

The position vector $\mathbf{o}_6$ of the origin O_6 of frame $\mathcal{F}_6$ in frame $\mathcal{F}_5$ is given by:

$$\mathbf{o}_6 = -l_0 \cos\alpha \, \mathbf{i}_5 + l_0 \sin\alpha \, \mathbf{j}_5 + 0 \, \mathbf{k}_5, \tag{11}$$

10

or, in the inertial frame $\mathcal{F}$:

$$\mathbf{o}_6 = (x_5 - l_0 \cos\theta_6)\,\mathbf{i} + (y_5 - l_0 \sin\theta_6)\,\mathbf{j} + r\,\mathbf{k}, \quad \text{with} \quad \theta_6 = \theta_5 - \alpha. \tag{12}$$

The absolute velocity $\mathbf{v}_6$ and absolute angular velocity $\boldsymbol{\omega}_6$ of the chassis, expressed in frame $\mathcal{F}_6$, are given by:

$$\mathbf{v}_6 = v_5 \cos\alpha\,\mathbf{i}_6 = \frac{r}{2}\cos\alpha(\dot\theta_1 + \dot\theta_2)\,\mathbf{i}_6, \tag{13}$$

$$\boldsymbol{\omega}_6 = \frac{1}{l_0}v_5 \sin\alpha\,\mathbf{k}_6 = \frac{r}{2l_0}\sin\alpha(\dot\theta_1 + \dot\theta_2)\,\mathbf{k}_6. \tag{14}$$

The position vector of the chassis $[x_6\ y_6\ \theta_6]^T$ can be derived from the relations:

$$\dot\theta_6 = \omega_6, \quad x_6 = x_5 - l_0\cos\theta_6, \quad y_6 = y_5 - l_0\sin\theta_6, \quad \text{with} \quad \theta_6 = \theta_5 - \alpha. \tag{15}$$

First epicyclic gear train - Front left wheel assembly (1)

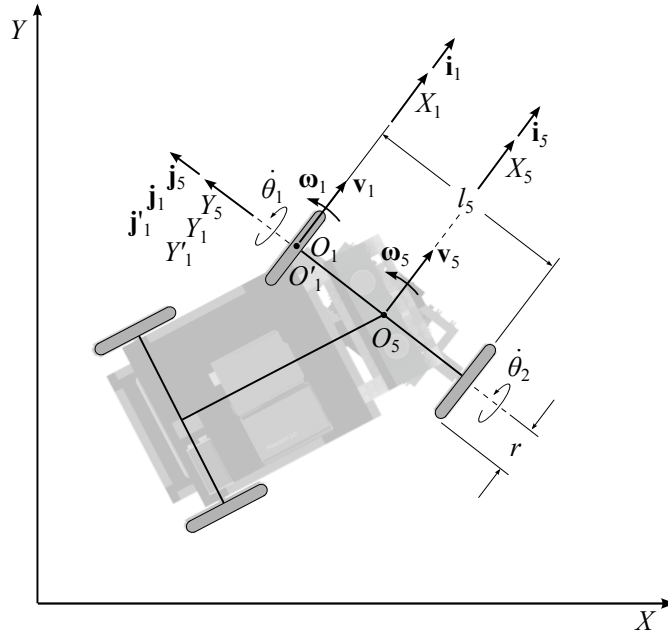The variables describing the kinematics of the front left wheel assembly are shown in Fig. 7.

Figure 7: Sketch for the kinematics of the front left wheel assembly

11

Let $\{O_1, X_1, Y_1, Z_1\}$ be the frame $\mathcal{F}_1$ attached to the planet-carrier, with origin O_1 located at the intersection of the midplane of the left front wheel and the axis of rotation of the same wheel. The position vector $\mathbf{o}_1$ of O_1 in frame $\mathcal{F}_5$ is given by:

$$\mathbf{o}_1 = 0\,\mathbf{i}_5 + \frac{l_5}{2}\,\mathbf{j}_5 + 0\,\mathbf{k}_5. \tag{16}$$

Furthermore, let $\{O_1', X_1', Y_1', Z_1'\}$ be the frame $\mathcal{F}_1'$ attached to the left front wheel, with origin O_1' coinciding with O_1. Let $\mathbf{Q}_1$ be the 3×3 orthogonal matrix that rotates frame $\mathcal{F}_1'$ with respect to the frame $\mathcal{F}_1$ around the Y_1 axis through an angle θ_1:

$$\mathbf{Q}_1 = \begin{bmatrix} \cos\theta_1 & 0 & \sin\theta_1 \\ 0 & 1 & 0 \\ -\sin\theta_1 & 0 & \cos\theta_1 \end{bmatrix}. \tag{17}$$

The absolute velocity $\mathbf{v}_1$ and absolute angular velocity $\boldsymbol{\omega}_1$ of the left front wheel assembly, expressed in frame $\mathcal{F}_1$, are given by:

$$\mathbf{v}_1 = r\dot{\theta}_1\,\mathbf{i}_1, \tag{18}$$

$$\boldsymbol{\omega}_1 = \dot{\theta}_1\,\mathbf{j}_1 + \omega_5\,\mathbf{k}_1 = \dot{\theta}_1\,\mathbf{j}_1 + \frac{r}{l_5}(\dot{\theta}_2 - \dot{\theta}_1)\,\mathbf{k}_1. \tag{19}$$

First epicyclic gear train - Lower left gear assembly (7)

The variables describing the kinematics of the lower left gear assembly are shown in Fig. 8. Let $\{O_7, X_7, Y_7, Z_7\}$ be the frame $\mathcal{F}_7$ attached to the planet-carrier, with origin O_7 located at the intersection of the axis of rotation the lower left gear and its center of mass. The position vector $\mathbf{o}_7$ of frame $\mathcal{F}_7$ in frame $\mathcal{F}_5$ is given by:

$$\mathbf{o}_7 = 0\,\mathbf{i}_5 + l_7\,\mathbf{j}_5 + (h_7 - r)\,\mathbf{k}_5, \tag{20}$$

where h_7 is the height of the center of mass of the lower left gear assembly. Furthermore, let $\{O_7', X_7', Y_7', Z_7'\}$ be the frame $\mathcal{F}_7'$ attached to the lower left gear, with origin O_7' coinciding with O_7. Let $\mathbf{Q}_7$ be the 3×3 orthogonal matrix that rotates frame $\mathcal{F}_7'$ with respect to frame
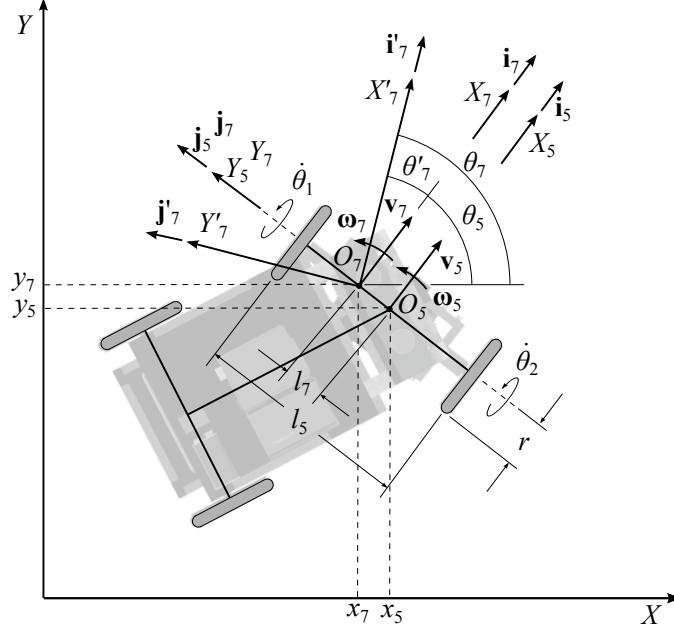
Figure 8: Sketch for the kinematics of the lower left gear assembly

$\mathcal{F}_7$ around the Z_7 axis through an angle θ'_7:

$$\mathbf{Q}_7 = \begin{bmatrix} \cos\theta'_7 & -\sin\theta'_7 & 0 \\ \sin\theta'_7 & \cos\theta'_7 & 0 \\ 0 & 0 & 1 \end{bmatrix} \tag{21}$$

with

$$\theta'_7 = \theta_7 - \theta_5, \quad \omega'_7 = \omega_7 - \omega_5. \tag{22}$$

Let $N_{1,7}$ denote the ratio of the number N_7 of teeth of gear 7 to the number N_1 of teeth of gear 1. This ratio is also the ratio of the angular velocity of the left wheel $\dot{\theta}_1$ to the angular velocity of the lower left gear assembly ω'_7, as observed in frame $\mathcal{F}_7$, which is

$$N_{1,7} = -\frac{\dot{\theta}_1}{\omega'_7}. \tag{23}$$

The lower left gear angular velocity ω'_7, observed in frame $\mathcal{F}_7$, is then

$$\omega'_7 = -\frac{1}{N_{1,7}}\dot{\theta}_1. \tag{24}$$

13

The absolute angular velocity of the lower left gear assembly $\boldsymbol{\omega}_7$ expressed in frame $\mathcal{F}_7$ is given by:

$$\boldsymbol{\omega}_7 = (\omega_5 + \omega_7') \, \mathbf{k}_7 = \left[\frac{r}{l_5}(\dot{\theta}_2 - \dot{\theta}_1) - \frac{1}{N_{1,7}}\dot{\theta}_1 \right] \mathbf{k}_7, \tag{25}$$

The absolute velocity of the lower left gear assembly $\mathbf{v}_7$ expressed in frame F_7 is given by:

$$\mathbf{v}_7 = (v_5 - l_7\omega_5) \, \mathbf{i}_7 = \left[\frac{r}{2}(\dot{\theta}_1 + \dot{\theta}_2) - \frac{r l_7}{l_5}(\dot{\theta}_2 - \dot{\theta}_1) \right] \mathbf{i}_7, \tag{26}$$

First epicyclic gear train - Inner sun gear assembly (9)

The variables describing the kinematics of the inner sun gear assembly are shown in Fig. 9.

Figure 9: Sketch for the kinematics of the inner sun gear assembly

Let $\{O_9, X_9, Y_9, Z_9\}$ be the frame $\mathcal{F}_9$ attached to the planet-carrier, with origin O_9 located at the intersection of the axis of the inner sun gear assembly and its center of mass. The orientation of frame $\mathcal{F}_9$ is the same as that of frame $\mathcal{F}_5$. The position vector $\mathbf{o}_9$ of frame $\mathcal{F}_9$ in frame $\mathcal{F}_5$ is given by

$$\mathbf{o}_9 = 0 \, \mathbf{i}_5 + 0 \, \mathbf{j}_5 + (h_9 - r) \, \mathbf{k}_5, \tag{27}$$

14

where h_9 is the height of the center of mass of the inner sun gear assembly. Furthermore, let $\{O'_9, X'_9, Y'_9, Z'_9\}$ be the frame $\mathcal{F}'_9$ attached to the inner sun gear assembly, with origin O'_9 coinciding with O_9. Let $\mathbf{Q}_9$ be the 3×3 orthogonal matrix that rotates frame $\mathcal{F}'_9$ with respect to the frame $\mathcal{F}_9$ around the Z_9 axis through an angle θ'_9:

$$\mathbf{Q}_9 = \begin{bmatrix} \cos\theta'_9 & -\sin\theta'_9 & 0 \\ \sin\theta'_9 & \cos\theta'_9 & 0 \\ 0 & 0 & 1 \end{bmatrix} \tag{28}$$

with

$$\theta'_9 = \theta_9 - \theta_5, \quad \omega'_9 = \omega_9 - \omega_5. \tag{29}$$

Let $N_{7,9}$ denote the ratio of the number N_9 of teeth of gear 9 to the number N_7 of teeth of gear 7. This ratio is also the ratio of the angular velocity of the lower left gear assembly ω'_7 to the angular velocity of the inner sun gear assembly ω'_9, as observed in frame $\mathcal{F}_5$, which is

$$N_{7,9} = -\frac{\omega'_7}{\omega'_9}. \tag{30}$$

Combining eqs. (23) and (30) yields:

$$\omega'_9 = +\frac{1}{N_{1,7}N_{7,9}}\dot{\theta}_1. \tag{31}$$

The absolute angular velocity of the inner sun gear assembly $\boldsymbol{\omega}_9$ expressed in frame $\mathcal{F}_9$ is given by:

$$\omega_9 = \omega_5 + \omega'_9 \tag{32}$$

$$\boldsymbol{\omega}_9 = \left[\frac{r}{l_5}(\dot{\theta}_2 - \dot{\theta}_1) + \frac{1}{N_{1,7}N_{7,9}}\dot{\theta}_1\right]\mathbf{k}_9 \tag{33}$$

The absolute velocity of the inner sun gear assembly $\mathbf{v}_9$ expressed in frame $\mathcal{F}_9$ is equal to the absolute velocity of the planet-carrier $\mathbf{v}_5$:

$$\mathbf{v}_9 = \frac{r}{2}(\dot{\theta}_1 + \dot{\theta}_2)\mathbf{i}_9. \tag{34}$$

We will also need the angular velocity of the inner sun gear assembly ω''_9 as observed in frame

15

$\mathcal{F}_6$ for the derivation of the angular velocity relations of the upper right gear assembly:

$$\omega_9'' = \omega_9 - \omega_6 = \omega_9' + \omega_5 - \omega_6 = \frac{1}{N_{1,7}N_{7,9}}\dot{\theta}_1 + \omega_5 - \omega_6. \tag{35}$$

First epicyclic gear train - Upper right gear assembly (11)

The variables describing the kinematics of the upper right gear assembly are shown in Fig. 10.
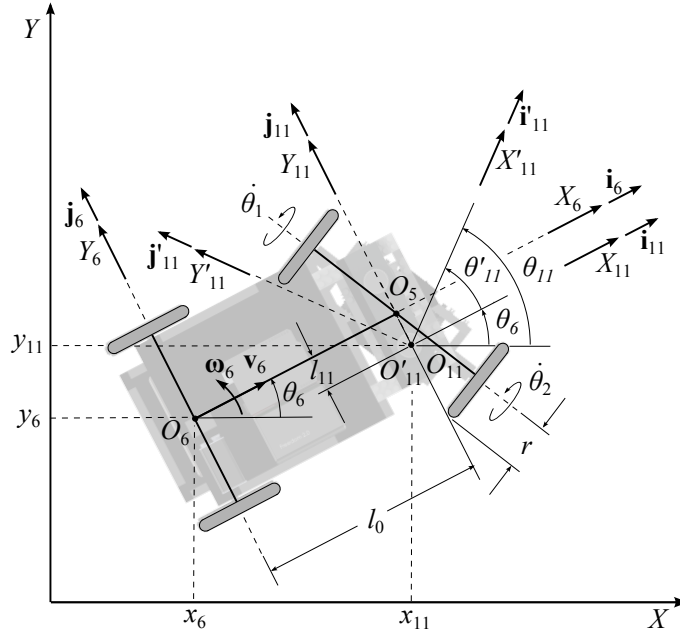

Figure 10: Sketch for the kinematics of the upper right gear assembly

Let $\{O_{11}, X_{11}, Y_{11}, Z_{11}\}$ be the frame $\mathcal{F}_{11}$ attached to the chassis, with origin O_{11} located at the intersection of the axis of the upper right gear assembly and its center of mass. The orientation of frame $\mathcal{F}_{11}$ is the same as that of frame $\mathcal{F}_6$ while the position vector $\mathbf{o}_{11}$ of O_{11} in frame $\mathcal{F}_6$ is given by:

$$\mathbf{o}_{11} = l_0\,\mathbf{i}_6 - l_{11}\,\mathbf{j}_6 + (h_{11} - r)\,\mathbf{k}_6, \tag{36}$$

where h_{11} is the height of the center of mass of the upper right gear assembly. Furthermore, let $\{O_{11}', X_{11}', Y_{11}', Z_{11}'\}$ be the frame $\mathcal{F}_{11}'$ attached to the upper right gear assembly, with O_{11}' coinciding with O_{11}. Let $\mathbf{Q}_{11}$ be the 3×3 orthogonal matrix that rotates frame $\mathcal{F}_{11}'$ with

respect to the frame $\mathcal{F}_{11}$ around the Z_{11} axis through an angle θ'_{11}:

$$\mathbf{Q}_{11} = \begin{bmatrix} \cos\theta'_{11} & -\sin\theta'_{11} & 0 \\ \sin\theta'_{11} & \cos\theta'_{11} & 0 \\ 0 & 0 & 1 \end{bmatrix}, \tag{37}$$

with

$$\theta'_{11} = \theta_{11} - \theta_6, \quad \omega'_{11} = \omega_{11} - \omega_6. \tag{38}$$

Let $N_{9,11}$ denote the ratio of the number N_{11} of teeth of gear 1 to the number N_9 of teeth of gear 9. This ratio is also the ratio of the angular velocity of the inner sun gear assembly ω''_9 to the angular velocity of the upper right gear assembly ω'_{11}, as observed in frame $\mathcal{F}_6$, which is

$$N_{9,11} = -\frac{\omega''_9}{\omega'_{11}}, \tag{39}$$

The angular velocity of the upper right gear assembly ω'_{11}, as observed in frame $\mathcal{F}_6$, is given by:

$$\omega'_{11} = -\frac{\omega''_9}{N_{9,11}} = -\frac{1}{N_{1,7}N_{7,9}N_{9,11}}\dot{\theta}_1 - \frac{1}{N_{9,11}}(\omega_5 - \omega_6) \tag{40}$$

The angular velocity of the upper right gear assembly ω'_{11}, as observed in frame $\mathcal{F}_6$, corresponds to the velocity sensing of motor 1, i.e.,

$$\omega'_{11} \equiv \omega_{m1}, \quad \omega_{m1} = -\frac{1}{N_{1,7}N_{7,9}N_{9,11}}\dot{\theta}_1 - \frac{1}{N_{9,11}}\dot{\alpha}. \tag{41}$$

The angular velocity of the left wheel $\dot{\theta}_1$ in terms of the velocity sensing of motor 1 is given by:

$$\dot{\theta}_1 = -N_{1,7}N_{7,9}N_{9,11}\left(\omega_{m1} + \frac{1}{N_{9,11}}\dot{\alpha}\right). \tag{42}$$

The absolute angular velocity of the upper left gear assembly $\boldsymbol{\omega}_{11}$ as observed in frame F_{11} is given by:

$$\omega_{11} = \omega_6 + \omega'_{11} = \omega_6 - \frac{1}{N_{1,7}N_{7,9}N_{9,11}}\dot{\theta}_1 - \frac{1}{N_{9,11}}(\omega_5 - \omega_6), \tag{43}$$

$$\boldsymbol{\omega}_{11} = \left[-\frac{1}{N_{1,7}N_{7,9}N_{9,11}}\dot{\theta}_1 + \left(1 + \frac{1}{N_{9,11}}\right)\frac{r}{2l_0}\sin\alpha(\dot{\theta}_1 + \dot{\theta}_2) - \frac{r}{l_5 N_{9,11}}(\dot{\theta}_2 - \dot{\theta}_1)\right]\mathbf{k}_{11}. \tag{44}$$

The absolute velocity of the upper left gear assembly $\mathbf{v}_{11}$ as observed in frame $\mathcal{F}_{11}$ is given by:

$$\mathbf{v}_{11} = (v_6 + l_{11}\omega_6)\,\mathbf{i}_{11} + l_0\omega_6\,\mathbf{j}_{11}, \tag{45}$$

$$\mathbf{v}_{11} = \left[\frac{r}{2}\cos\alpha(\dot{\theta}_1 + \dot{\theta}_2) + \frac{rl_{11}}{2l_0}\sin\alpha(\dot{\theta}_1 + \dot{\theta}_2)\right]\mathbf{i}_{11} + \frac{r}{2}\sin\alpha(\dot{\theta}_1 + \dot{\theta}_2)\,\mathbf{j}_{11}, \tag{46}$$

Second epicyclic gear train - Front right wheel assembly (2)

The variables describing the kinematics of the front right wheel assembly are shown in Fig. 11.
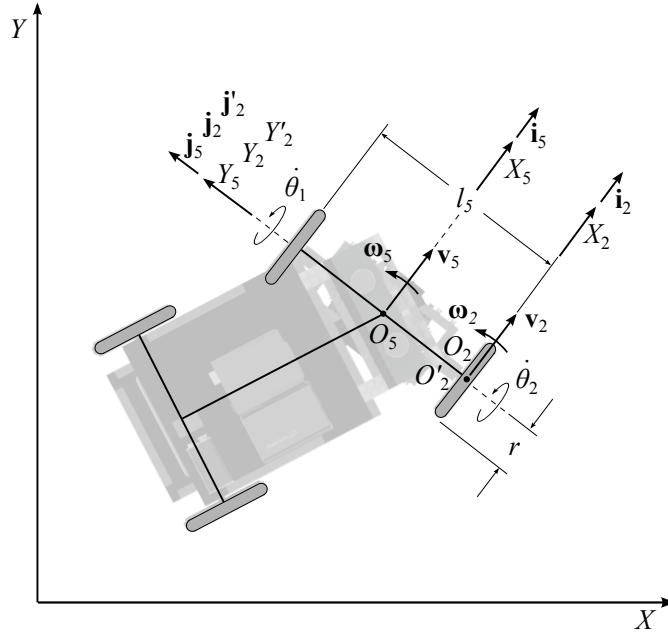
Figure 11: Sketch for the kinematics of the front right wheel assembly

Let $\{O_2, X_2, Y_2, Z_2\}$ be the frame $\mathcal{F}_2$ attached to the planet-carrier, with origin O_2 located at the intersection of the midplane of the right front wheel and the axis of rotation of the same wheel. The orientation of frame $\mathcal{F}_2$ is the same as that of frame $\mathcal{F}_5$ while the position

18

vector $\mathbf{o}_2$ of the origin of frame $\mathcal{F}_2$ in frame $\mathcal{F}_5$ is given by:

$$\mathbf{o}_2 = 0\,\mathbf{i}_5 - \frac{l_5}{2}\,\mathbf{j}_5 + 0\,\mathbf{k}_5. \tag{47}$$

Furthermore, let $\{O'_2, X'_2, Y'_2, Z'_2\}$ be the frame $\mathcal{F}'_2$ attached to the right front wheel, with origin O'_2 coinciding with O_2. Let $\mathbf{Q}_2$ be the 3×3 orthogonal matrix that rotates frame $\mathcal{F}'_2$ with respect to frame $\mathcal{F}_2$ around the Y_2 axis through an angle θ_2:

$$\mathbf{Q}_2 = \begin{bmatrix} \cos\theta_2 & 0 & \sin\theta_2 \\ 0 & 1 & 0 \\ -\sin\theta_2 & 0 & \cos\theta_2 \end{bmatrix}. \tag{48}$$

The absolute velocity $\mathbf{v}_2$ and absolute angular velocity $\boldsymbol{\omega}_2$ of the front right wheel assembly expressed in frame $\mathcal{F}_2$ are given by:

$$\mathbf{v}_2 = r\dot{\theta}_2\,\mathbf{i}_2, \tag{49}$$

$$\boldsymbol{\omega}_2 = \dot{\theta}_2\,\mathbf{j}_2 + \omega_5\,\mathbf{k}_2 = \dot{\theta}_2\,\mathbf{j}_2 + \frac{r}{l_5}(\dot{\theta}_2 - \dot{\theta}_1)\,\mathbf{k}_2. \tag{50}$$

Second epicyclic gear train - Lower right gear assembly (8)

The variables describing the kinematics of the lower right gear assembly are shown in Fig. 12. Let $\{O_8, X_8, Y_8, Z_8\}$ be the frame $\mathcal{F}_8$ attached to the planet-carrier, with origin O_8 located at the intersection of the axis of the lower right gear assembly and its center of mass. The orientation of frame $\mathcal{F}_8$ is the same as that of frame $\mathcal{F}_5$, while the position vector $\mathbf{o}_8$ of the origin O_8 of frame $\mathcal{F}_8$ with respect to frame $\mathcal{F}_5$ is given by:

$$\mathbf{o}_8 = 0\,\mathbf{i}_5 - l_8\,\mathbf{j}_5 + (h_8 - r)\,\mathbf{k}_5, \tag{51}$$

where h_8 is the height of the center of mass of the lower right gear assembly. Furthermore, let $\{O'_8, X'_8, Y'_8, Z'_8\}$ be the frame $\mathcal{F}'_8$ attached to the lower right gear, with origin O'_8 coinciding with O_8. Let $\mathbf{Q}_8$ be the 3×3 orthogonal matrix that rotates frame $\mathcal{F}'_8$ with respect to the
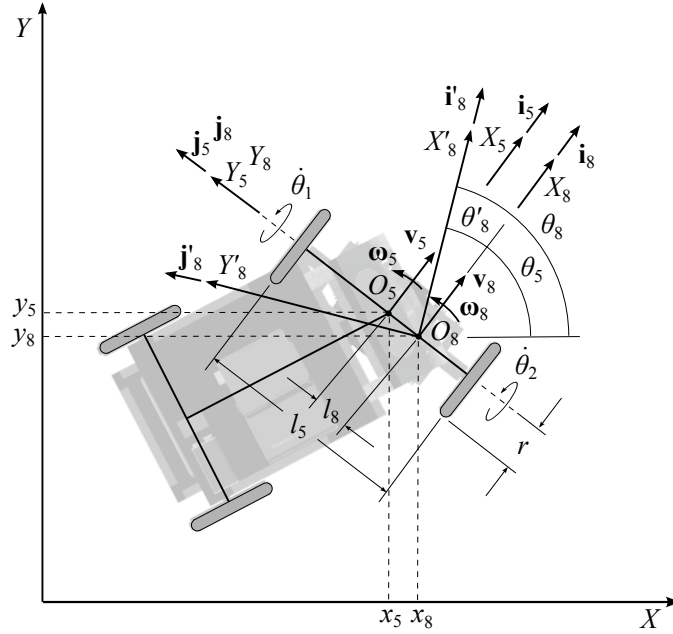
Figure 12: Kinematics of the lower left gear assembly

frame $\mathcal{F}_8$ around the Z_8 axis through an angle θ_8':

$$\mathbf{Q}_8 = \begin{bmatrix} \cos\theta_8' & -\sin\theta_8' & 0 \\ \sin\theta_8' & \cos\theta_8' & 0 \\ 0 & 0 & 1 \end{bmatrix}, \tag{52}$$

with

$$\theta_8' = \theta_8 - \theta_5, \quad \omega_8 = \omega_5 + \omega_8'. \tag{53}$$

Let $N_{2,8}$ denote the ratio of the number N_8 of teeth of gear 8 to the number N_2 of teeth of gear 2. This ratio is also the ratio of the angular velocity of the right wheel $\dot{\theta}_2$ to the angular velocity of the lower right gear assembly ω_8', as observed in frame $\mathcal{F}_8$:

$$N_{2,8} = +\frac{\dot{\theta}_2}{\omega_8'}. \tag{54}$$

Then, the lower right gear angular velocity ω_8' observed in frame $\mathcal{F}_8$ is defined as:

$$\omega_8' = +\frac{1}{N_{2,8}}\dot{\theta}_2. \tag{55}$$

20

The absolute angular velocity of the lower right gear assembly $\boldsymbol{\omega}_8$ expressed in frame $\mathcal{F}_8$ is defined by:

$$\boldsymbol{\omega}_8 = (\omega_5 + \omega_8') \, \mathbf{k}_8 = \left(\frac{r}{l_5}(\dot{\theta}_2 - \dot{\theta}_1) + \frac{1}{N_{2,8}}\dot{\theta}_2 \right) \mathbf{k}_8 \tag{56}$$

The absolute velocity of the lower right gear assembly $\mathbf{v}_8$, expressed in frame $\mathcal{F}_8$ is defined by:

$$\mathbf{v}_8 = (v_5 + l_8\omega_5) \, \mathbf{i}_8 = \left(\frac{r}{2}(\dot{\theta}_1 + \dot{\theta}_2) + \frac{rl_8}{l_5}(\dot{\theta}_2 - \dot{\theta}_1) \right) \mathbf{i}_8, \tag{57}$$

Second epicyclic gear train - Outer sun gear assembly (10)

The variables describing the kinematics of the outer sun gear assembly are shown in Fig. 13.

Figure 13: Sketch for the kinematics of the outer sun gear assembly

Let $\{O_{10}, X_{10}, Y_{10}, Z_{10}\}$ be the frame $\mathcal{F}_{10}$ attached to the planet-carrier, with origin O_{10} located at the intersection of the axis of the outer sun gear assembly and its center of mass. The orientation of frame $\mathcal{F}_{10}$ is the same as that of frame $\mathcal{F}_5$ while the position vector $\mathbf{o}_{10}$

of the origin of frame $\mathcal{F}_{10}$ in frame $\mathcal{F}_5$ is given by:

$$\mathbf{o}_8 = 0\,\mathbf{i}_5 + 0\,\mathbf{j}_5 + (h_{10} - r)\,\mathbf{k}_5. \tag{58}$$

where h_{10} is the height of the center of mass of the outer sun gear assembly. Furthermore, let $\{O'_{10}, X'_{10}, Y'_{10}, Z'_{10}\}$ be the frame $\mathcal{F}'_{10}$ attached to the outer sun gear assembly, with origin O'_{10} coinciding with O_{10}. Let $\mathbf{Q}_{10}$ be the 3×3 orthogonal matrix that rotates frame $\mathcal{F}'_{10}$ with respect to frame $\mathcal{F}_{10}$ around the Z_{10} axis through an angle θ'_{10}:

$$\mathbf{Q}_{10} = \begin{bmatrix} \cos\theta'_{10} & -\sin\theta'_{10} & 0 \\ \sin\theta'_{10} & \cos\theta'_{10} & 0 \\ 0 & 0 & 1 \end{bmatrix} \tag{59}$$

with

$$\theta_{10} = \theta_5 + \theta'_{10}, \quad \omega_{10} = \omega_5 + \omega'_{10}. \tag{60}$$

Let $N_{8,10}$ denote the ratio of the number N_{10} of teeth of gear 10 to the number N_8 of teeth of gear 8. This ratio is also the ratio of the angular velocity of the lower right gear assembly ω'_8 to the angular velocity of the outer sun gear assembly ω'_{10} as observed in frame $\mathcal{F}_5$:

$$N_{8,10} = -\frac{\omega'_8}{\omega'_{10}}. \tag{61}$$

Combining equations (54) and (61) yields:

$$\omega'_{10} = -\frac{1}{N_{2,8}N_{8,10}}\dot{\theta}_2. \tag{62}$$

The absolute angular velocity of the outer sun gear assembly $\boldsymbol{\omega}_{10}$ expressed in frame $\mathcal{F}_{10}$ is given by:

$$\omega_{10} = \omega_5 + \omega'_{10} = \frac{r}{l_5}(\dot{\theta}_2 - \dot{\theta}_1) - \frac{1}{N_{2,8}N_{8,10}}\dot{\theta}_2, \tag{63}$$

$$\boldsymbol{\omega}_{10} = \left[-\frac{r}{l_5}\dot{\theta}_1 + \left(\frac{r}{l_5} - \frac{1}{N_{2,8}N_{8,10}} \right)\dot{\theta}_2 \right]\mathbf{k}_{10}. \tag{64}$$

The absolute velocity of the outer sun gear assembly $\mathbf{v}_{10}$ expressed in frame $\mathcal{F}_{10}$ is equal to

the absolute velocity of the planet-carrier $\mathbf{v}_5$:

$$\mathbf{v}_{10} = \frac{r}{2}(\dot{\theta}_1 + \dot{\theta}_2)\,\mathbf{i}_{10}. \tag{65}$$

We will also need the angular velocity of the outer sun gear assembly ω_{10}'' as observed in frame $\mathcal{F}_6$ for the derivation of the angular velocity equations of the upper left gear assembly:

$$\omega_{10}'' = \omega_{10} - \omega_6 = \omega_{10}' + \omega_5 - \omega_6 = -\frac{1}{N_{2,8}N_{8,10}}\dot{\theta}_2 + \omega_5 - \omega_6. \tag{66}$$

Second epicyclic gear train - Upper left gear assembly (12)

The variables describing the kinematics of the upper left gear assembly are shown in Fig. 14.
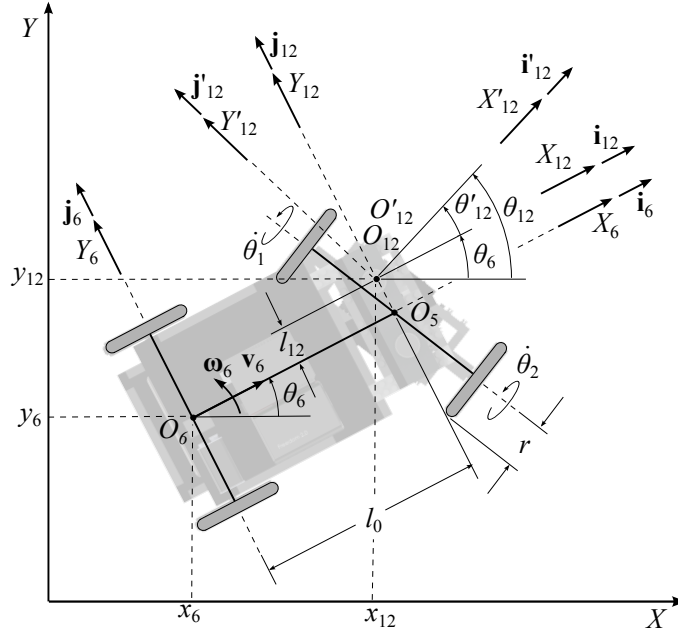
Figure 14: Sketch for the kinematics of the upper left gear assembly

Let $\{O_{12}, X_{12}, Y_{12}, Z_{12}\}$ be the frame $\mathcal{F}_{12}$ attached to the chassis, with origin O_{12} located at the intersection of the axis of the upper left gear assembly and its center of mass. The orientation of frame $\mathcal{F}_{12}$ is the same as that of frame $\mathcal{F}_5$ while the position vector $\mathbf{o}_{12}$ of the

23

origin of frame $\mathcal{F}_{12}$ in frame $\mathcal{F}_6$ is given by:

$$\mathbf{o}_{12} = l_0\,\mathbf{i}_6 + l_{12}\,\mathbf{j}_6 + (h_{12} - r)\,\mathbf{k}_6, \tag{67}$$

where h_{12} is the height of the center of mass of the upper left gear assembly. Furthermore, let $\{O'_{12}, X'_{12}, Y'_{12}, Z'_{12}\}$ be the frame $\mathcal{F}'_{12}$ attached to the upper left gear assembly, with origin O'_{12} coiciding with O_{12}. Let $\mathbf{Q}_{12}$ be the 3×3 orthogonal matrix that rotates frame $\mathcal{F}'_{12}$ with respect to the frame $\mathcal{F}_{12}$ around the Z_{12} axis through an angle θ'_{12}:

$$\mathbf{Q}_{12} = \begin{bmatrix} \cos\theta'_{12} & -\sin\theta'_{12} & 0 \\ \sin\theta'_{12} & \cos\theta'_{12} & 0 \\ 0 & 0 & 1 \end{bmatrix}, \tag{68}$$

with

$$\theta'_{12} = \theta_{12} - \theta_6, \quad \omega'_{12} = \omega_{12} - \omega_6. \tag{69}$$

Let $N_{10,12}$ denote the ratio of the number N_{12} of teeth of gear 12 to the number N_{10} of teeth of gear 10. This ratio is also the ratio of the angular velocity of the outer sun gear assembly ω''_{10} to the angular velocity of the upper left gear assembly ω'_{12}, as observed in frame $\mathcal{F}_6$:

$$N_{10,12} = -\frac{\omega''_{10}}{\omega'_{12}}, \tag{70}$$

The angular velocity of the upper left gear assembly ω'_{12}, as observed in frame $\mathcal{F}_6$, is given by:

$$\omega'_{12} = -\frac{\omega''_{10}}{N_{10,12}} = \frac{1}{N_{2,8}N_{8,10}N_{10,12}}\dot{\theta}_2 - \frac{1}{N_{10,12}}(\omega_5 - \omega_6), \tag{71}$$

The angular velocity of the upper left gear assembly ω'_{12}, as observed in frame $\mathcal{F}_6$, corresponds to the velocity sensing of motor 2:

$$\omega'_{12} \equiv \omega_{m2}, \quad \omega_{m2} = \frac{1}{N_{2,8}N_{8,10}N_{10,12}}\dot{\theta}_2 - \frac{1}{N_{10,12}}\dot{\alpha}. \tag{72}$$

The angular velocity of the right wheel $\dot{\theta}_2$ in terms of the velocity sensing of motor 2 is given by:

$$\dot{\theta}_2 = N_{2,8}N_{8,10}N_{10,12}\left(\omega_{m2} + \frac{1}{N_{10,12}}\dot{\alpha}\right). \tag{73}$$

The absolute angular velocity of the upper left gear assembly $\boldsymbol{\omega}_{12}$ as observed in frame $\mathcal{F}_{12}$ is given by:

$$\omega_{12} = \omega_6 + \omega'_{12} = \omega_6 + \frac{1}{N_{2,8}N_{8,10}N_{10,12}}\dot{\theta}_2 - \frac{1}{N_{10,12}}(\omega_5 - \omega_6), \tag{74}$$

$$\boldsymbol{\omega}_{12} = \left[\frac{1}{N_{2,8}N_{8,10}N_{10,12}}\dot{\theta}_2 + \left(1 + \frac{1}{N_{10,12}}\right)\frac{r}{2l_0}\sin\alpha(\dot{\theta}_1 + \dot{\theta}_2) - \frac{r}{l_5 N_{10,12}}(\dot{\theta}_2 - \dot{\theta}_1)\right]\mathbf{k}_{12}. \tag{75}$$

The absolute velocity of the upper left gear assembly $\mathbf{v}_{12}$ as observed in frame $\mathcal{F}_{12}$ is given by:

$$\mathbf{v}_{12} = (v_6 - l_{12}\omega_6)\,\mathbf{i}_{12} + l_0\omega_6\,\mathbf{j}_{12}, \tag{76}$$

or, upon substitution of the various velocities involved,

$$\mathbf{v}_{12} = \left[\frac{r}{2}\cos\alpha(\dot{\theta}_1 + \dot{\theta}_2) - \frac{rl_{12}}{2l_0}\sin\alpha(\dot{\theta}_1 + \dot{\theta}_2)\right]\mathbf{i}_{12} + \frac{r}{2}\sin\alpha(\dot{\theta}_1 + \dot{\theta}_2)\,\mathbf{j}_{12}. \tag{77}$$

Rear left wheel assembly (3)

The variables describing the kinematics of the rear left wheel assembly are shown in Fig. 15. Let $\{O_3, X_3, Y_3, Z_3\}$ be the frame $\mathcal{F}_3$ attached to the chassis, with origin O_3 located at the intersection of the midplane of the rear left wheel and the axis of rotation of the same wheel. The orientation of frame $\mathcal{F}_3$ is the same as that of frame $\mathcal{F}_6$. The position vector $\mathbf{o}_3$ of the origin of frame $\mathcal{F}_3$ in frame $\mathcal{F}_6$ is given by:

$$\mathbf{o}_3 = 0\,\mathbf{i}_6 + \frac{l_6}{2}\,\mathbf{j}_6 + 0\,\mathbf{k}_6. \tag{78}$$

Furthermore, let $\{O'_3, X'_3, Y'_3, Z'_3\}$ be the frame $\mathcal{F}'_3$ attached to the rear left wheel assembly, with O'_3 coinciding with O_3. Let $\mathbf{Q}_3$ be the 3×3 orthogonal matrix that rotates frame $\mathcal{F}'_3$ with respect to frame $\mathcal{F}_3$ around the Y_3 axis through an angle θ_3:

$$\mathbf{Q}_3 = \begin{bmatrix} \cos\theta_3 & 0 & \sin\theta_3 \\ 0 & 1 & 0 \\ -\sin\theta_3 & 0 & \cos\theta_3 \end{bmatrix}. \tag{79}$$
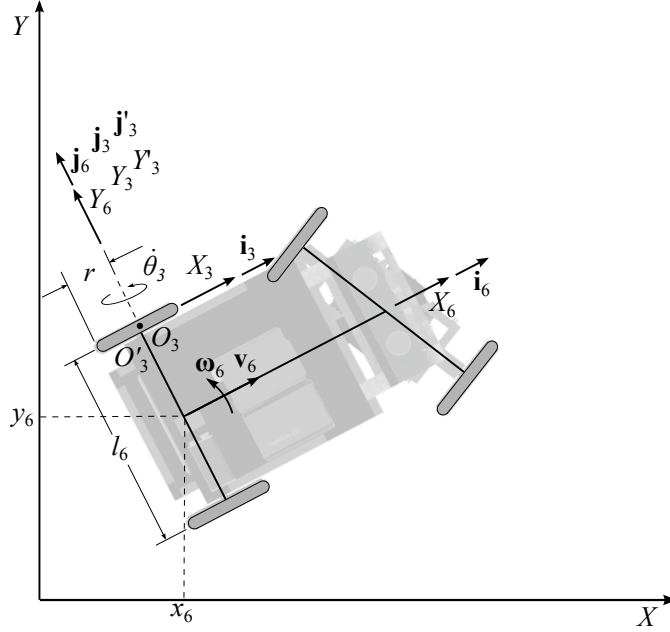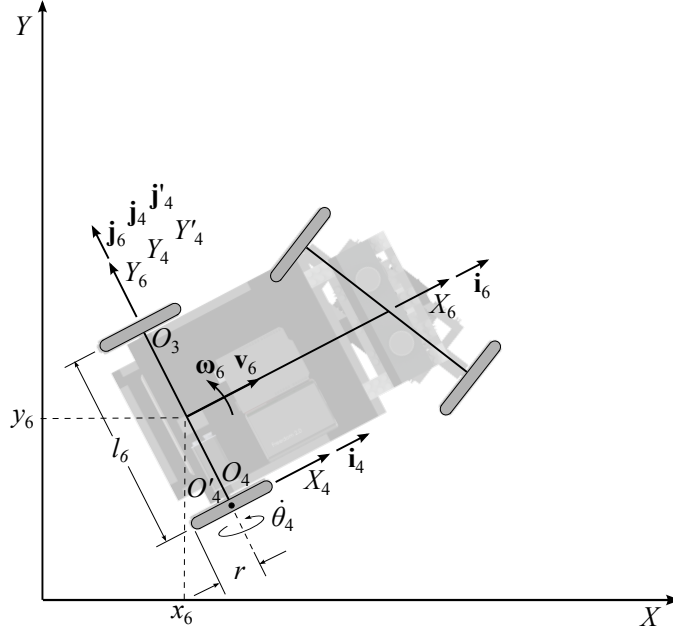
Figure 15: Sketch for the kinematics of the rear left wheel assembly

The absolute velocity of the rear left wheel assembly $\mathbf{v}_3$, as observed in frame $\mathcal{F}_3$, is given by:

$$\mathbf{v}_3 = \left(v_6 - \frac{l_6}{2}\omega_6 \right) \mathbf{i}_3 = \left[\frac{r}{2} \cos\alpha(\dot\theta_1 + \dot\theta_2) - \frac{rl_6}{4l_0} \sin\alpha(\dot\theta_1 + \dot\theta_2) \right] \mathbf{i}_3. \tag{80}$$

The absolute angular velocity of the rear left wheel assembly $\boldsymbol{\omega}_3$, observed in frame $\mathcal{F}_3$, is given by:

$$\boldsymbol{\omega}_3 = \frac{v_3}{r}\,\mathbf{j}_3 + \omega_6\,\mathbf{k}_3, \tag{81}$$

$$\boldsymbol{\omega}_3 = \left[\frac{1}{2}\cos\alpha(\dot\theta_1 + \dot\theta_2) - \frac{l_6}{4l_0}\sin\alpha(\dot\theta_1 + \dot\theta_2) \right] \mathbf{j}_3 + \frac{r}{2l_0}\sin\alpha(\dot\theta_1 + \dot\theta_2)\,\mathbf{k}_3. \tag{82}$$

Rear right wheel assembly (4)

The variables describing the kinematics of the rear right wheel assembly are shown in Fig. 16. Let $\{O_4, X_4, Y_4, Z_4\}$ be the frame $\mathcal{F}_4$ attached to the chassis, with origin O_4 located at the intersection of the midplane of the rear right wheel and the axis of rotation of the same

26

Figure 16: Sketch for the kinematics of the rear right wheel assembly

wheel. The orientation of frame $\mathcal{F}_4$ is the same as that of frame $\mathcal{F}_6$. The position vector $\mathbf{o}_4$ of the origin of frame $\mathcal{F}_4$ in frame $\mathcal{F}_6$ is given by:

$$\mathbf{o}_4 = 0\,\mathbf{i}_6 - \frac{l_6}{2}\,\mathbf{j}_6 + 0\,\mathbf{k}_6. \tag{83}$$

Furthermore, let $\{O_4', X_4', Y_4', Z_4'\}$ be the frame $\mathcal{F}_4'$ attached to the rear right wheel assembly, with origin O_4' coinciding with O_4. Let $\mathbf{Q}_4$ be the 3×3 orthogonal matrix that rotates frame $\mathcal{F}_4'$ with respect to the frame $\mathcal{F}_4$ around the Y_4 axis through an angle θ_4:

$$\mathbf{Q}_4 = \begin{bmatrix} \cos\theta_4 & 0 & \sin\theta_4 \\ 0 & 1 & 0 \\ -\sin\theta_4 & 0 & \cos\theta_4 \end{bmatrix}. \tag{84}$$

The absolute velocity of the rear right wheel assembly $\mathbf{v}_4$ observed in frame $\mathcal{F}_4$ is given by:

$$\mathbf{v}_4 = \left(v_6 + \frac{l_6}{2}\omega_6\right)\mathbf{i}_4 = \left[\frac{r}{2}\cos\alpha(\dot{\theta}_1 + \dot{\theta}_2) + \frac{l_6 r}{4l_0}\sin\alpha(\dot{\theta}_1 + \dot{\theta}_2)\right]\mathbf{i}_4. \tag{85}$$

27

The absolute angular velocity of the rear right wheel assembly $\boldsymbol{\omega}_4$ observed in frame $\mathcal{F}_4$ is given, in turn, by:

$$\boldsymbol{\omega}_4 = \frac{v_4}{r}\,\mathbf{j}_4 + \omega_6\,\mathbf{k}_4, \tag{86}$$

$$\boldsymbol{\omega}_4 = \left[\frac{1}{2}\cos\alpha(\dot{\theta}_1 + \dot{\theta}_2) + \frac{l_6}{4l_0}\sin\alpha(\dot{\theta}_1 + \dot{\theta}_2)\right]\mathbf{j}_4 + \frac{r}{2l_0}\sin\alpha(\dot{\theta}_1 + \dot{\theta}_2)\,\mathbf{k}_4. \tag{87}$$

2.2 Dynamics

The dynamics model of the mechanical system under study is of the general form [5]:

$$\mathbf{I}\ddot{\boldsymbol{\theta}}_a + \mathbf{C}\dot{\boldsymbol{\theta}}_a = \boldsymbol{\tau}, \tag{88}$$

with

$$\boldsymbol{\tau} \equiv \begin{bmatrix} \tau_1 & \tau_2 \end{bmatrix}^T, \tag{89}$$

while $\mathbf{I}$ is the 2×2 generalized inertia matrix, $\mathbf{C}$ is the 2×2 the generalized matrix of Coriolis and centrifugal forces and $\boldsymbol{\tau}$ is the vector of torques delivered to the two front wheels.

In deriving the equations of motion, we distinguish between the output torque of the motors which we call the *motor torques* and the torque that is delivered to the wheels which we call the *wheel torques*. We define the vector of motor torques as:

$$\boldsymbol{\tau}_m \equiv \begin{bmatrix} \tau'_1 & \tau'_2 \end{bmatrix}^T, \tag{90}$$

where τ'_1 and τ'_2 are the torques delivered by the two motors. The torques are related through equation:

$$\tau_1 = -N_{1,m1}\tau'_1, \quad N_{1,m1} \equiv N_{1,7}N_{7,9}N_{9,11}, \tag{91}$$

$$\tau_2 = N_{2,m2}\tau'_2, \quad N_{2,m2} \equiv N_{2,8}N_{8,10}N_{10,12}, \tag{92}$$

The wheel torques are used to derive the equations of motion of the robot.

The expression for the generalized inertia matrix $\mathbf{I}$ is derived from the kinetic energy of the ith rigid body, namely:

$$T_i = \frac{1}{2}\mathbf{t}_i^T\mathbf{M}_i\mathbf{t}_i, \tag{93}$$

where $\mathbf{M}_i$ is the constant 6×6 *inertia dyad* of the ith rigid body defined in terms of the 3×3 inertia matrix $\mathbf{J}_i$ and the mass m_i of the ith rigid body:

$$\mathbf{M}_i \equiv \begin{bmatrix} \mathbf{J}_i & \mathbf{0}_{3\times 3} \\ \mathbf{0}_{3x3} & m_i\mathbf{1}_{3\times 3} \end{bmatrix}, \quad \mathbf{J}_i \equiv \begin{bmatrix} J_{xi} & 0 & 0 \\ 0 & J_{yi} & 0 \\ 0 & 0 & J_{zi} \end{bmatrix} \tag{94}$$

where $\mathbf{J}_i$ is expressed in the same reference frame as the twist $\mathbf{t}_i$ of the ith rigid body.

Upon introduction of relations (4), the above expression becomes

$$T_i = \frac{1}{2}\dot{\boldsymbol{\theta}}_a^T(\mathbf{T}_i^T\mathbf{M}_i\mathbf{T}_i)\dot{\boldsymbol{\theta}}_a, \tag{95}$$

a quadratic form in the vector of wheel rates, whose matrix is the *inertia matrix* of the ith body, namely,

$$\mathbf{I}_i = \mathbf{T}_i^T\mathbf{M}_i\mathbf{T}_i. \tag{96}$$

The inertia matrix of the overall mechanical system is simply the sum of all 12 body-matrices of inertia:

$$\mathbf{I} = \sum_{i=1}^{12}\mathbf{T}_i^T\mathbf{M}_i\mathbf{T}_i, \tag{97}$$

The generalized matrix of the Coriolis and centrifugal forces $\mathbf{C}_i$, associated with the ith body, is defined as:

$$\mathbf{C}_i = \mathbf{T}_i^T\mathbf{M}_i\dot{\mathbf{T}}_i + \mathbf{T}_i^T\mathbf{W}_i\mathbf{M}_i\mathbf{T}_i, \tag{98}$$

while the system counterpart matrix is simply the sum of all 12 body-matrices $\mathbf{C}_i$, i.e.,

$$\mathbf{C} = \sum_{i=1}^{12}(\mathbf{T}_i^T\mathbf{M}_i\dot{\mathbf{T}}_i + \mathbf{T}_i^T\mathbf{W}_i\mathbf{M}_i\mathbf{T}_i), \tag{99}$$

with $\dot{\mathbf{T}}_i$ denoting the time-derivative of the 6×2 twist-shaping matrix of the ith rigid body

and $\mathbf{W}_i$ is the 6×6 *angular velocity dyad* of the ith rigid body, which is given by:

$$\mathbf{W}_i \equiv \begin{bmatrix} \mathbf{\Omega}_i & \mathbf{0}_{3\times 3} \\ \mathbf{0}_{3\times 3} & \mathbf{0}_{3\times 3} \end{bmatrix}, \quad \mathbf{\Omega}_i \equiv \begin{bmatrix} 0 & -\omega_{zi} & \omega_{yi} \\ \omega_{zi} & 0 & -\omega_{xi} \\ -\omega_{yi} & \omega_{xi} & 0 \end{bmatrix}. \tag{100}$$

Since $\boldsymbol{\omega}_i$ is a function of α and $\dot{\boldsymbol{\theta}}_a$, $\mathbf{W}_i$ is also a function of α and $\dot{\boldsymbol{\theta}}_a$:

$$\mathbf{W} \equiv \mathbf{W}(\alpha, \dot{\boldsymbol{\theta}}_a) \tag{101}$$

For some of the 12 assemblies, namely, the rear left wheel, the rear right wheel, the chassis, the upper left gear and the upper right gear assemblies, the twist-shaping matrices $\mathbf{T}_i$ are functions of α. Their time differentiation $\dot{\mathbf{T}}_i$ then becomes a function of α and $\dot{\alpha}$, i.e.,

$$\dot{\mathbf{T}}_i = \dot{\mathbf{T}}_i(\alpha, \dot{\alpha}) \tag{102}$$

However, $\dot{\alpha}$ is a function of α and $\dot{\boldsymbol{\theta}}_a$, namely,

$$\dot{\alpha} = \omega_5 - \omega_6 \quad \Rightarrow \quad \dot{\alpha} = \frac{r}{l_5}(\dot{\theta}_2 - \dot{\theta}_1) - \frac{r}{2l_0}(\dot{\theta}_1 + \dot{\theta}_2)\sin\alpha. \tag{103}$$

Using eq.(103) the time-derivative of the twist-shaping matrix of the ith rigid body $\dot{\mathbf{T}}_i$ can now be expressed as a function of α and $\dot{\boldsymbol{\theta}}_a$:

$$\dot{\mathbf{T}}_i \equiv \dot{\mathbf{T}}_i(\alpha, \dot{\boldsymbol{\theta}}_a) \tag{104}$$

For the other assemblies, namely, the front left wheel, the front right wheel, the chassis, the lower left gear, the lower right gear, the inner sun gear and the outer sun gear, the twist-shaping matrices are constant so their time differentiation equals zero.

The mathematical model of the robot thus reduces to:

$$\boldsymbol{\tau} = \mathbf{I}(\alpha)\ddot{\boldsymbol{\theta}}_a + \mathbf{C}(\alpha, \dot{\boldsymbol{\theta}}_a)\dot{\boldsymbol{\theta}}_a, \tag{105}$$

where $\mathbf{I}(\alpha)$ and $\mathbf{C}(\alpha, \dot{\boldsymbol{\theta}}_a)$ are defined as:

$$\mathbf{I}(\alpha) = \sum_{i=1}^{12} \mathbf{T}_i(\alpha)^T \mathbf{M}_i \mathbf{T}_i(\alpha) \tag{106}$$

$$\mathbf{C}(\alpha, \dot{\boldsymbol{\theta}}_a) = \sum_{i=1}^{12} \left[\mathbf{T}_i(\alpha)^T \mathbf{M}_i \dot{\mathbf{T}}_i(\alpha, \dot{\boldsymbol{\theta}}_a) + \mathbf{T}_i(\alpha)^T \mathbf{W}_i(\alpha, \dot{\boldsymbol{\theta}}_a) \mathbf{M}_i \mathbf{T}_i(\alpha) \right]. \tag{107}$$

Note here that the term $\mathbf{C}(\alpha, \dot{\boldsymbol{\theta}}_a) \dot{\boldsymbol{\theta}}_a$ clearly shows the quadratic nature of the generalized Coriolis and centrifugal terms with respect to the joint rates. As the foregoing generalized matrix arises from the presence of α, only the rear left wheel, the rear right wheel, the chassis, the upper left gear and the upper right gear assemblies contribute to this term. Furthermore, since the chassis, the upper left gear and the upper right gear assemblies undergo planar motion, only the two rear wheel assemblies contribute to the term $\mathbf{T}_i^T \mathbf{W}_i \mathbf{M}_i \mathbf{T}_i$ [5].

The inertial and mass parameters of each of the 12 rigid-body assemblies are derived using SolidWorks, with the mass density of the Acrylonitrile Butadiene Styrene (ABS) LEGO parts and the stainless steel modified axles, and by weighing the other parts of the robot (battery, motors, mechatronics). The mass of the motors is included in the mass of the chassis assembly while the inertia of the 2 motor rotors is added to the corresponding upper gear assemblies. The total mass of the robot was also compared to the total simulated mass of the robot under SolidWorks to validate the model. Finally, the equations of motion of the robot were derived in terms of the 12 rigid body assemblies using Maple.

The evaluated generalized inertia matrix $\mathbf{I}(\alpha)$ is given by:

$$\mathbf{I}(\alpha) = \begin{bmatrix} I_{1,1} & I_{1,2} \\ I_{1,2} & I_{2,2} \end{bmatrix}, \tag{108}$$

$$I_{1,1} = (0.751213 + 0.170970 \cos 2\alpha - 0.021247 \sin \alpha) \times 10^{-3},$$
$$I_{1,2} = (0.576631 + 0.170970 \cos 2\alpha) \times 10^{-3},$$
$$I_{2,2} = (0.751894 + 0.170970 \cos 2\alpha + 0.021246 \sin \alpha) \times 10^{-3},$$

all with units of $\mathrm{Kg} \cdot \mathrm{m}^2$. We note here the symmetry of the generalized inertia matrix. The

entries of the generalized inertia matrix are shown in Appendix A. Because of the difference in mass and inertia of the inner and outer sun gear assemblies, the inertia matrix terms $I_{1,1}$ and $I_{2,2}$ are different. The effort needed to accelerate the robot is higher at an angle α of 0 and π corresponding to forward and reverse motion of the robot than the effort needed to accelerate the robot at an angle α of $\pi/2$ and $3\pi/4$ corresponding to a pure rotation of the chassis.

The evaluated matrix of generalized Coriolis and centrifugal fores $\mathbf{C}(\alpha)$ is given by:

$$\mathbf{C}(\alpha, \dot{\boldsymbol{\theta}}_a) = \begin{bmatrix} C_{1,1} & C_{1,1} \\ C_{2,2} & C_{2,2} \end{bmatrix}, \tag{109}$$

$$\begin{aligned} C_{1,1} &= (3.48117 \sin 2\alpha + 1.20648 \cos \alpha - 0.99401 \cos 3\alpha) \times 10^{-5} \dot{\theta}_1 \\ &+ (0.78154 \cos \alpha - 0.99401 \cos 3\alpha - 3.35764 \sin 2\alpha) \times 10^{-5} \dot{\theta}_2, \\ C_{2,2} &= (3.35764 \sin 2\alpha + 0.78154 \cos \alpha - 0.99401 \cos 3\alpha) \times 10^{-5} \dot{\theta}_1 \\ &+ (1.20648 \cos \alpha - 0.99401 \cos 3\alpha - 3.48117 \sin 2\alpha) \times 10^{-5} \dot{\theta}_2, \end{aligned}$$

all with units of $\mathrm{Kg} \cdot \mathrm{m}^2/\mathrm{s}$.

Using the equations of motion derived in this section, we can now proceed to the definition of a control algorithm.

3 Control

Our aim here is to design a controller using pole-placement and state-feedback while taking into account that the robot is configuration-dependent in terms of α.

3.1 State-Space Form

The first step in defining a proper control is to express the equations of motion of the system in state-space form [6], [7]. We define the state vector of the system as

$$\mathbf{x} \equiv \dot{\boldsymbol{\theta}}_a = \begin{bmatrix} \dot{\theta}_1 & \dot{\theta}_2 \end{bmatrix}^T. \tag{110}$$

while the desired state vector is defined as

$$\mathbf{x}_d \equiv \begin{bmatrix} \dot{\theta}'_1 & \dot{\theta}'_2 \end{bmatrix}^T, \tag{111}$$

where $\dot{\theta}'_1$ and $\dot{\theta}'_2$ are the desired actuated joint rates of the robot.

The controlled variables are defined as the velocity and angular velocity of the planet-carrier assembly, ω_5 and v_5. We thus define the desired output vector $\mathbf{y}_d$, also known as the reference input vector of our system, as

$$\mathbf{y}_d \equiv \begin{bmatrix} v'_5 & \omega'_5 \end{bmatrix}^T, \tag{112}$$

the actual output vector of the system being

$$\mathbf{y} \equiv \begin{bmatrix} v_5 & \omega_5 \end{bmatrix}^T. \tag{113}$$

We can express the reference input vector $\mathbf{y}_d$ and the actual output vector $\mathbf{y}$ as linear transformations of the desired state vector and the state vector, respectively, with:

$$\mathbf{y}_d = \mathbf{H}\mathbf{x}_d, \quad \mathbf{y} = \mathbf{H}\mathbf{x}, \quad \mathbf{H} = \begin{bmatrix} \dfrac{r}{2} & \dfrac{r}{2} \\ -\dfrac{r}{l_5} & \dfrac{r}{l_5} \end{bmatrix} \tag{114}$$

where $\mathbf{H}$ is the state output matrix.

The dynamics model of the mechanical system is given by

$$\mathbf{I}(\alpha)\ddot{\boldsymbol{\theta}}_a + \mathbf{C}(\alpha, \dot{\boldsymbol{\theta}}_a)\dot{\boldsymbol{\theta}}_a = \boldsymbol{\tau}. \tag{115}$$

Solving for $\ddot{\boldsymbol{\theta}}_a$ from the above model yields:

$$\ddot{\boldsymbol{\theta}}_a = -\mathbf{I}^{-1}(\alpha)\mathbf{C}(\alpha, \dot{\boldsymbol{\theta}}_a)\dot{\boldsymbol{\theta}}_a + \mathbf{I}^{-1}(\alpha)\boldsymbol{\tau}. \tag{116}$$

The dynamics model can then be expressed in state-space form as:

$$\dot{\mathbf{x}} = \mathbf{l}(\mathbf{x}, \mathbf{u}), \quad \mathbf{y} = \mathbf{H}\mathbf{x}, \tag{117}$$

with

$$\mathbf{u} \equiv \begin{bmatrix} \tau_1 & \tau_2 \end{bmatrix}^T, \quad \mathbf{l}(\mathbf{x}, \mathbf{u}) = -\mathbf{I}^{-1}(\alpha)\mathbf{C}(\alpha, \mathbf{x})\mathbf{x} + \mathbf{I}^{-1}(\alpha)\mathbf{u}, \tag{118}$$

where $\mathbf{u}$ is the input vector of the system.

3.2   Model Linearization

In order to linearize the state space model, we resort to Lyapunov's linearization method (LLM) [6]. To do this, we linearize the model around an equilibrium state by setting

$$\mathbf{l}(\mathbf{x}, \mathbf{u}) = \mathbf{0}_2, \quad \text{with} \quad \mathbf{u}_0 = \mathbf{0}_2, \quad \mathbf{x}_0 = \mathbf{0}_2, \tag{119}$$

where $\mathbf{0}_k$ is the k-dimensional zero vector. This state represents the robot at rest.

Linearizing the state-space model at the equilibrium state yields

$$\dot{\mathbf{x}} = \mathbf{F}\mathbf{x} + \mathbf{G}\mathbf{u}, \quad \mathbf{y} = \mathbf{H}\mathbf{x}, \tag{120}$$

with

$$\mathbf{F} \equiv \left. \frac{\partial \mathbf{l}}{\partial \mathbf{x}} \right|_{\mathbf{x}=\mathbf{x}_0} = \mathbf{O}_{2\times2}, \quad \mathbf{G} \equiv \left. \frac{\partial \mathbf{l}}{\partial \mathbf{u}} \right|_{\mathbf{x}=\mathbf{x}_0} = \mathbf{I}^{-1}(\alpha), \tag{121}$$

where $\mathbf{F}$ is the state matrix and $\mathbf{G}$ is the input matrix of the system.

Note here that linearizing the model at a rest state is equivalent to neglecting the generalized matrix of the Coriolis and centrifugal forces that arises from the presence of $\dot{\alpha}$.

3.3   Open-Loop System

In order to design a controller using pole placement, the open-loop system is first analyzed in the s-domain of the Laplace Transform. The open-loop poles of the linearized equations of motion are the eigenvalues of the system matrix $\mathbf{F}$:

$$\mathbf{p} = \mathrm{eig}(\mathbf{F}) = \mathrm{eig}(\mathbf{O}_{2\times 2}), \tag{122}$$

whence the two open-loop poles of the system are $\{0,0\}$ and, as expected, the open-loop system is marginally stable (poles are on the imaginary axis), because dissipative forces are not included in the model.

3.4   State Feedback

We now derive the state feedback control law based on pole-placement. We want the closed-loop poles of the system to be located in the left half of the s-plane. To this end, we use a control law of the form:

$$\mathbf{u} = -\mathbf{Kx}. \tag{123}$$

where $\mathbf{K}$ is the 2×2 state feedback matrix, which affects the location of the closed-loop poles [6]. Substituting the feedback law given by Eq.(123) into the system described by Eq.(120) yields

$$\dot{\mathbf{x}} = \mathbf{Fx} - \mathbf{GKx}. \tag{124}$$

The block diagram for the control law of the system is shown in Fig. 17.
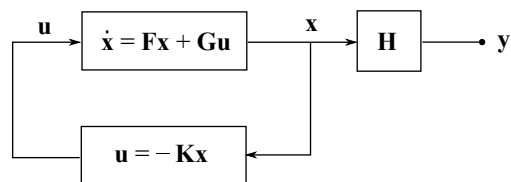
Figure 17: Block diagram for the control law of the system

The closed-loop poles of the system correspond to the eigenvalues of system (124):

$$\mathbf{p} = \text{eig}(\mathbf{F} - \mathbf{GK}), \tag{125}$$

Moreover, we introduce a gain matrix, which adapts to the configuration parameter α:

$$\mathbf{K} \equiv \rho \mathbf{I}(\alpha). \tag{126}$$

which leads to the characteristic equation

$$(s + \rho)(s + \rho) = 0. \tag{127}$$

Therefore, the two closed-loop poles of the system are located on the real axis at $\{-\rho, -\rho\}$. By selecting $\rho > 0$, the closed-loop poles are placed on the left-hand side of the complex plane, thereby keeping the system stable. Furthermore, the dominant poles of the closed-loop system are designed to be real so as to have an aperiodic time response. We end up with a control law that adapts to α. By adjusting ρ we can tune the time-response to the desired output vector $\mathbf{y}_d$ of the system. We need to find a proper balance between the performance of the system and the effort of the actuators. A higher ρ corresponds to poles farther to the left in the s-plane and to a faster time-response combined with a higher torque required from the motors.

3.5 Reference Input

The shape of the state feedback control law allowing reference tracking is

$$\mathbf{u} = -\mathbf{Kx} + \mathbf{Ny}_d, \quad \mathbf{N} = (\mathbf{N}_u + \mathbf{KN}_x) \tag{128}$$

where $\mathbf{N}$ is the gain matrix that guarantees a reference input tracking [6]. The bloc diagram for the control law of the system with reference tracking is shown in Fig. 18. Matrices $\mathbf{N}_x$ and $\mathbf{N}_u$ are given below in block-form [7]:

$$\mathbf{D} \begin{bmatrix} \mathbf{N}_x \\ \mathbf{N}_u \end{bmatrix} = \begin{bmatrix} \mathbf{0}_{2\times2} \\ \mathbf{1}_{2\times2} \end{bmatrix}, \quad \mathbf{D} = \begin{bmatrix} \mathbf{F} & \mathbf{G} \\ \mathbf{H} & \mathbf{O}_{2\times2} \end{bmatrix}, \tag{129}$$
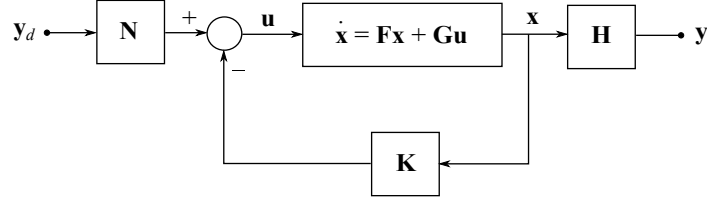
Figure 18: Bloc diagram for the control law of the system with reference tracking

where $\mathbf{D}$ is required to be invertible. While $\mathbf{F} = \mathbf{O}_{2\times2}$, but since $\mathbf{G}$ and $\mathbf{H}$ are invertible, $\mathbf{D}$ can be shown to be invertible as well. Indeed, by means of a swapping of the two left-hand blocks of $\mathbf{D}$ with their right-hand counterparts, a block diagonal matrix is obtained, whose determinant is the product of the determinants of its two diagonal blocks. Hence, the gain matrices become

$$\mathbf{N}_u = \mathbf{0}_{2\times2}, \quad \mathbf{N}_x = \mathbf{H}^{-1}, \quad \mathbf{N} = \mathbf{KH}^{-1}. \tag{130}$$

The state feedback control then follows:

$$\mathbf{u} = -\mathbf{Kx} + \mathbf{KH}^{-1}\mathbf{y}_d, \tag{131}$$

or, equivalently,

$$\mathbf{u} = \mathbf{K}(\mathbf{H}^{-1}\mathbf{y}_d - \mathbf{x}), \quad \mathbf{u} = \mathbf{K}(\mathbf{x}_d - \mathbf{x}). \tag{132}$$

The simplified bloc diagram for the control law of the system with reference tracking is shown in Fig. 19.
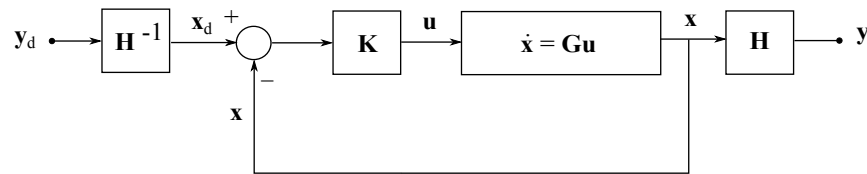
Figure 19: Simplified bloc diagram for the control law of the system with reference tracking

3.6 Simulation Runs

In order to validate the controller and analyze the dynamic performance of the system, simulation runs were conducted using Simulink. The model is shown in Fig. 20.
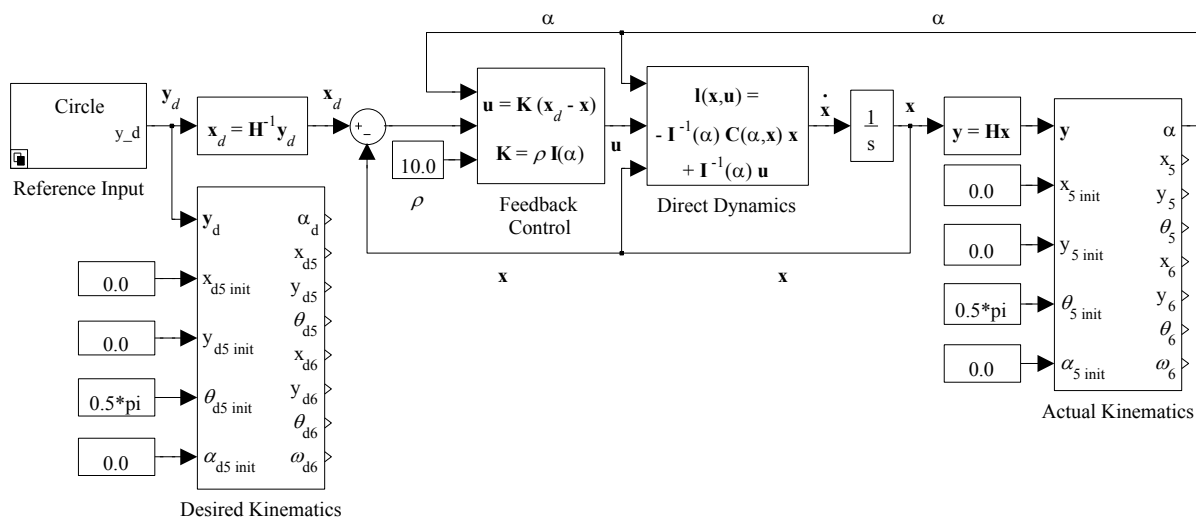

Figure 20: Simulink model

The model uses the configuration-dependent feedback control and the state-space equations of the system. The direct dynamics block is a "Variant Subsystem Block" and can be switched between full state-space dynamics and linearized state-space dynamics. As mentioned earlier, the linearized system is equivalent to neglecting the generalized matrix of Coriolis and centrifugal forces that arises from the presence of $\dot{\alpha}$.

The actual and desired kinematics of the planet-carrier and the chassis are included in the model. The two blocks use the reference input vector $\mathbf{y}_d$ and the output vector $\mathbf{y}$ to derive the kinematic variables. The two blocks use the kinematic equations described in this report. The values are integrated over time from the initial position of the robot. The inside of the kinematics block is shown in Fig. 21.

The model needs the initial coordinates of the planet-carrier, $x_{5\ \text{init}}$ and $y_{5\ \text{init}}$, its initial angle, $\theta_{5\ \text{init}}$, and the initial angle between the planet-carrier and the chassis, α_{init}. The initial position of the robot is shown in Fig. 22. Note that the 3D position of all 12 moving assemblies could be determined in this manner using the kinematic equations described in
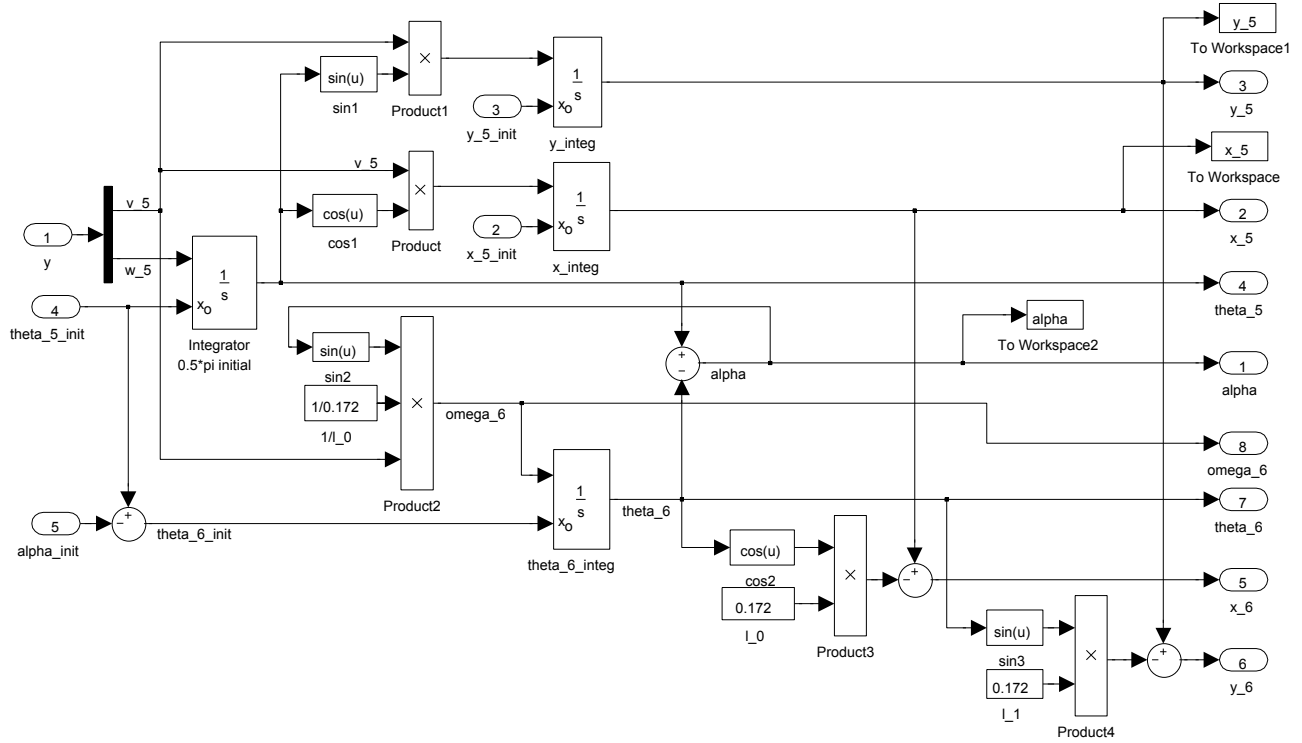
this report.

Figure 21: Simulink kinematics block

The reference input block outputs the desired planet-carrier velocity v_{d5} and angular velocity ω_{d5} combined in the reference input vector $\mathbf{y}_{d5}$. The state output matrix $\mathbf{H}$ is used to transform the desired planet-carrier velocity v_{d5} and angular velocity ω_{d5} to the desired left and right wheel angular velocities, $\dot{\theta}_{d1}$ and $\dot{\theta}_{d2}$.

Five different reference inputs were implemented: step-input trajectory, straight trajectory, rotation of the planet-carrier trajectory, circle trajectory and parking trajectory. These can be selected using the reference input "Variant Subsystem Block". The trajectories can be modified inside the blocks by adjusting different parameters such as the amplitude, the maximum velocity, the maximum acceleration, the task time, the trajectory angle, etc. The straight trajectory, rotation of the planet-carrier trajectory and circle trajectory were implemented using 4-5-6-7 degree polynomials whereas the parking trajectory was implemented using a cycloidal path.
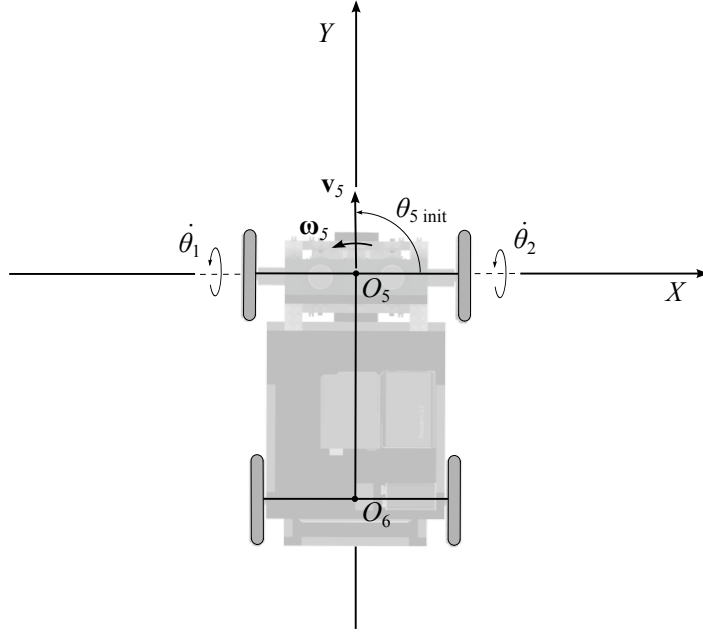
39

Figure 22: Initial position of the robot in the Simulink model; $x_{5\,\text{init}} = 0$ m; $y_{5\,\text{init}} = 0$ m; $\theta_{5\,\text{init}} = \pi/2$ rad; $\alpha_{\,\text{init}} = 0$ rad.

The gain ρ can be adjusted inside the model. As mentioned earlier, adjusting ρ tunes the time-response to the desired output vector $\mathbf{y}_d$ of the system. A higher ρ corresponds to higher wheel torques, τ_1 and τ_2, and a decreased wheel velocity and path error. For the step-input, we can use the maximum allowed wheel torque and the initial velocity error to find the maximum allowed gain parameter ρ. For the other reference inputs, the maximum torque will depend on the maximum trajectory acceleration. The gain parameter ρ can be higher for these reference inputs and will ultimately depend on the discrete time-domain implementation.

The desired wheel angular velocities, $\dot{\theta}_{d1}$ and $\dot{\theta}_{d2}$, are saturated in the Simulink model. The prototype was designed to be driven at a maximum of 1.0 m/s. With a wheel radius of 0.040 m, the maximum angular velocity of the wheels is thus 25.0 rad/s. The desired wheel torques, τ_1 and τ_2, are also saturated in the Simulink model. The maximum continuous motor rotor torque of the two motors is 0.00606 Nm. With a planetary gearhead gear ratio is 19:1 (3249:169), the maximum motor shaft torque is 0.1165 Nm. Finally, with a DWT gear ratio of 1:1, the maximum wheel torque is 0.1165 Nm.

The Simulink model outputs the variables to the MATLAB workspace. A post-load MATLAB function runs automatically after each run. It reads the variables from the MATLAB workspace and outputs a figure with the results of the simulation.

Results for the five different reference inputs are shown in Appendix B. Limits of the different parameters are shown on the figures. The results show that the configuration-dependent feedback controller is appropriate for the system and allows for an aperiodic time response.

In particular, for the step-input, the torque limit is respected by setting $\rho = 2.78$ s^{-1}. Also, as expected, the torque required for the rotation of the planet-carrier is much lower than the one required for the straight path trajectory since most of the weight is in the chassis. Part of the deviations from the circle trajectory and the parking trajectory arise from the presence of the matrix of generalized Coriolis and centrifugal forces. The feedback controller underestimates the torque required to compensate the presence of $\dot{\alpha}$.
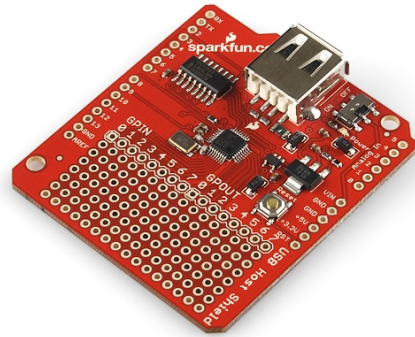
4   Mechatronics

We now describe the mechatronics system of the robot prototype.

The motors used for the prototype are two 21-V RE-Max Maxon motors (model number 221031). These are coupled to GP22A Maxon planetary gearheads (model number 110338) and Maxon magnetic quadrature encoders (model number 201937) with 512 counts per turn and 2 output channels.

We use the Arduino platform to implement the wireless control of the DWT prototype. Arduino is an open-source electronics prototyping platform. The Arduino Uno board, shown in Fig. 23a, is used as the main component of our mechatronics system. The Arduino Uno is a 8-bit microcontroller that is programmed with the Arduino software using the Arduino language, similar to the C language. The board can connect to a computer via a USB port. The robot control program is uploaded via this USB port. The port also allows a serial output while the program is running. This allows for data-collection via USB for simulation.
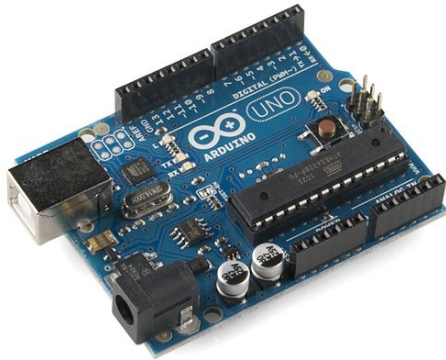
(a)   (b)

Figure 23: (a) Arduino Uno (b) USB host shield

The Arduino platform allows the stacking of electronic shields on top of the Arduino Uno to add functionality to the mechatronics system. The Arduino Uno and the shields have input and output pins to communicate, send and read signals. There are 14 input/output digital pins numbered from 0 to 13 and six analog input/output pins numbered from A0 to A5 available. We use three shields on top of the Arduino Uno for the wireless control of the two motors. The Arduino Uno requires a 9-V supply voltage available either from a standard 9-V battery or via a 9-V wall adapter.

(a)   (b)

Figure 24: (a) Logitech Freedom 2.4 cordless joystick (b) Receiver

The first shield is a USB host shield from Sparkfun. It allows the Arduino Uno to read data from a joystick wirelessly. The USB host shield is shown in Fig. 23b. We also use a

Freedom 2.4 cordless joystick from Logitech, shown in Fig. 24a. It communicates wirelessly with a USB receiver, shown in Fig. 24b. The receiver is connected via a USB port to the USB host shield. The shield allows the Arduino Uno to read the position of the joystick and the state of its 10 buttons. The joystick and buttons are used to control the robot. The joystick requires 3 AA batteries to operate.
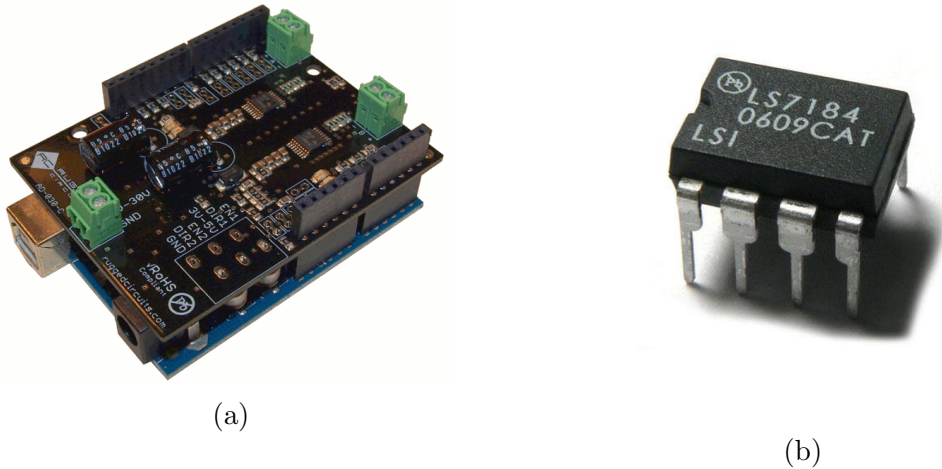

(a)

(b)

Figure 25: (a) Rugged motor driver shield (b) LS7184 encoder-to-counter interface chip

The second shield is a motor driver shield from Rugged Circuits, shown in Fig. 25a. It incorporates two Texas Instruments DRV8801 interface chips. These are motor drivers that allow pulse-width modulation (PWM) control of the two motors. It is capable of peak output currents of up to 2.8 A and operating voltages up to 36 V, which is enough for the two 21-V Maxon motors. It also allows current reading for feedback on the two DC motors. The connections of the shield were rewired to desired input and output pins of the Arduino Uno, which has also been modified to increase the sensitivity to current by removing two of the three resistors on the current output reading electronics. The Arduino Uno sends PWM signals, from 0 V to 5 V, to the motor drive shield through two pins along with two high or low digital signals for the motor voltage sign. These are then converted to voltage outputs by the motor drive for the motors. The standard PWM output frequency of the Arduino board, which has to be modified in the program in order to control the motors, was set to 31.25 kHz. A 22.2-V battery by ThunderPower (model number TP2250-6SP30) is connected to the motor drive in order to power the two motors.

The third shield is a custom shield that incorporates two LS7184 encoder-to-counter interface chips, shown in Fig. 25b. The shield is used to route the Arduino Uno 5-V supply voltage and ground to the two Maxon encoders and to the two LS7184 encoder chips. The two chips convert the A and B quadrature output of the motor encoders to a clock output and an up or down output. The Arduino Uno uses its two available external interrupt input pins and two digital input pins to read these two signals. We use an interrupt routine on the Arduino Uno to increase or decrease the encoder count each time there is a tick received from the LS7184 chips.

The Arduino program runs every 50 ms. The interrupt routine and the encoder count on each motor allow the determination of the speed of each motor rotor. These speed values are then converted to motor shaft speeds and wheel angular velocities using the equations described in Section 2.1. The wheel angular velocities are used to determine the actual planet-carrier velocity and angular velocity, besides the actual kinematics of the robot.

The Arduino program reads the joystick position and converts it to a desired reference input. The joystick Y position is used as the desired planet-carrier velocity and the joystick X position is used as the desired planet-carrier angular velocity. Button 1 on the joystick has to be pressed for the reference input to work. The reference inputs of the straight trajectory, planet-carrier rotation trajectory, circle trajectory and parking trajectory are also implemented on the Arduino program. These can be run by pressing buttons 7, 8, 9 or 10 on the joystick.

Using both the desired and actual planet-carrier velocity and angular velocity, we use the configuration-dependent feedback control to determine the desired wheel torques. These are then converted to motor shaft torques and then motor rotor torques.

Open-loop control is also implemented using the desired planet-carrier acceleration and angular acceleration. The open-loop control uses the inverted inertia matrix (neglecting the matrix of generalized Coriolis and centrifugal forces) and the desired wheel accelerations to determined the desired wheeled torques, rotor shaft torques and motor rotor torques. This control was implemented for the straight trajectory, rotation of the planet-carrier trajectory

and the circle trajectory. The parking trajectory could not be implemented because the acceleration equations were too long for the Arduino software.

The initial planned setup was to use a proportional-integral (PI) control scheme on the motor current, but the missing current sensing sign made this setup impossible to implement.

A closed-loop voltage control scheme was implemented instead. Using the desired torque τ and the motor torque constant K_τ, we obtain the desired motor current i. The electrical resistance of the system R is then used to obtain the torque voltage V_τ. The back-EMF voltage V_{emf} is calculated using the motor speed constant K_{emf} and the motor rotor speed $\dot{\phi}$. The error on the motor speed $\dot{\phi}_{error}$ is integrated and multiplied by an integral constant K_i to get the integral voltage term $V_\int$. All the voltage terms are then added to get the voltage output to the motors. The closed-loop voltage equations are

$$V_\tau = iR = \tau K_\tau R, \tag{133}$$

$$V_{emf} = \dot{\phi} K_{emf}, \tag{134}$$

$$V_\int = K_i \sum_{j=1}^{k} \dot{\phi}_{error}(t_i) \Delta t, \tag{135}$$

$$V = V_\tau + V_{emf} + V_\int \tag{136}$$

where V_τ, V_{emf}, $V_\int$ and V have units of V, K_τ has units of N/A, R has units of ohm, i has units of A, $\dot{\phi}$ and $\dot{\phi}_{error}$ have units of rpm, K_{emf} has units of V/rpm, K_i has units of V/rpm·s and Δt has units of s.

Throughout the Arduino program, saturation is applied to the desired wheel angular velocities, the desired torques, the desired currents, the desired voltages and the desired PWM outputs. This is done to limit the output voltage errors in the program and protect the motors from high voltages and currents.

Finally, a MATLAB program allows the capture of data from the Arduino board via a wired USB connection.

5   Recommendations for Future Work

Recommendations for future work on the Arduino platform includes:

- Possibly changing from the Arduino Uno board to the Arduino Mega board. The memory on the Arduino Uno is almost full for the current implementation, which does not leave much room to further develop the robot. The Arduino Mega board could be used with minor adjustments to the hardware currently used. It has four times the Arduino Uno memory.

- An Arduino compatible Wi-Fi shield was purchased for this robot prototype. But as a new product based on Arduino's open platform, there is a lack of software libraries to implement the wireless control of the prototype from a computer, possibly from within a Simulink and a MATLAB program. Possible improvements in software libraries available could allow this improvement. The Wi-Fi shield would replace the USB shield that allows for wireless joystick control. The joystick would be connected to the computer who would then send data wirelessly to the Wi-Fi shield.

Recommendations for future work on the dynamics and control includes:

- Modifying the inertia matrix to see if the configuration dependent control is suitable for small changes in the geometrical or inertial parameters of the robot.

- Exploring the control of the velocity and the angular velocity of the chassis. This has been done theoretically by Michalek [8] for similar robots with two actuated wheels and a trailer. This would be achieved with a control block that inputs the desired velocity and angular velocity of the chassis and outputs a corresponding desired velocity and angular velocity of the planet-carrier. It could also allow for the rear wheels of the robot to be leading in a trajectory (reverse motion).

- Implementing complex trajectories with obstacle patterns to showcase the maneuverability and mobility of the robot.

- Modeling friction and dissipative forces by adding a compensation to the input torque based on an estimator in the Simulink model and on the mechatronics platform. For the prototype described in this report, friction came from the two parts joining the

46

planet-carrier and the chassis, at the junction of the two front wheels and the planet-carrier and at the junction of the two rear wheels and the chassis.

- Including gear backlash in the Simulink model and the mechatronics platform. Considering the number of gears between the motors and the wheels, there is a considerable backlash error between the encoder reading and the actual wheel position. Modelling and including backlash would lessen the error in wheel position and path following.

- Doing a SimMechanics model of the robot in Simulink to confirm the validity of the kinematic and dynamic equations of the model and a 3D VRML model to allow 3D visualization of the Simulation. SolidWorks can export the 12 moving assemblies as single parts with their inertia in SimMechanics format which can then be assembled using frames, positions and rotations to relate forces on the parts and their dynamic response. SolidWorks can also export the 12 moving assemblies to the Simulink 3D VRML environment.

Recommendations for a future version of the robot includes:

- Trying a design with added mass and inertia in the planet-carrier. The relatively small mass and inertia of the planet-carrier, as compared to the chassis, makes it difficult to control. Adding mass and inertia to the planet-carrier could help in the control of the robot.

- Finding different vehicle applications in industry where the DWT could replace present transmissions and make a prototype resembling the actual design in order to show possible improvements in manoeuvrability and mobility. This would help the transfer of the DWT robot to industrial applications.

- Using an encoder on angle α to properly measure the position of the chassis relative to the planet-carrier and adapt the gains of the controller accordingly. In the current prototype, the angle α is integrated over time from the initial position and the kinematic equations of the robot. An encoder on angle α could also be used with an algorithm controlling the velocity and angular velocity of the chassis.

- Using servocontrollers for better torque tracking. Maxon Motors sells small servocontrollers that are compatible with the actual motors of the robot.

- Selecting a faster microcontroller with Simulink and MATLAB compatibility. The Arduino platform does not allow full compatibility and communication with Simulink and MATLAB. Simulink can convert block diagrams to C code and upload it on compatible microcontrollers that can then run hardware-in-the-loop (HIL) simulations. This would greatly lower the time spent on programming. The current design requires doing twice the work on both the Simulink platform and the Arduino platform. Some microcontrollers also allow wireless communication capability with Simulink and MATLAB, via Bluetooth for exemple. An example of such a prototyping platform is used for mobile robots at the University of Hagen in Germany using Texas Instruments C2000 microcontroller boards [9].

6 Conclusions

The control of a wheeled mobile robot with dual wheel transmission was discussed in this report. We first described the robot prototype, its transmission and its 12 moving assemblies. We derived the kinematic equations in terms of the twist of each assembly. We then described the dynamic equations of the robot in terms of the acceleration of the two actuated wheels and the configuration parameter α. The inertial and mass parameters, evaluated using SolidWorks, and the geometric parameters of the prototype were then used to define the dynamic equations of the robot in Maple. The state-space form of the system was used along with pole-placement to define a feedback controller for the configuration-dependent robot model. Simulation runs were performed under Simulink to validate the controller and analyze the dynamic performance of the system. The mechatronics implementation using the Arduino platform was then described. Finally, recommendations for future work were proposed.

References

[1] J. Angeles, "Driving and transmission unit for use in rolling vehicles," U.S Patent 6 948 576, Sep. 27, 2005.

[2] A. M. A. Husseini, "Mathematical modelling and mechatronic design of a mobile robot with a dual-wheel transmission," Honours B. Eng. Thesis, Department of Mechanical Engineering & Centre for Intelligent Machines, McGill University, Montreal, Oct. 2009.

[3] B. Pavlov, "Dual-wheel transmission robot - mathematical model validation," Final-year Project, Department of Mechanical Engineering & Centre for Intelligent Machines, McGill University, Montreal, Apr. 2010.

[4] W. Y. E. Mak, "Mechatronics implementation of a robot with dual wheel transmission," M. Eng. Project, Department of Mechanical Engineering & Centre for Intelligent Machines, McGill University, Montreal, Jan. 2012.

[5] J. Angeles, *Fundamentals of Robotic Mechanical Systems. Theory, Methods, and Algorithms*, 3rd ed. New York: Springer, 2007.

[6] A. Salerno and J. Angeles, "The control of semi-autonomous self-balancing two-wheeled quasiholonomic mobile robots," in *Proc. 15th CISM-IFToMM Symposium on Robot Design, Dynamics and Control (RoManSy 2004)*, Montreal, Canada, Jun. 2004.

[7] G. F. Franklin, J. D. Powell, and A. Emami-Naeini, *Feedback Control of Dynamics Systems*, 6th ed. Upper Saddle River, New Jersey: Prentice Hall, 2009.

[8] M. Michalek, "Geometrically motivated set-point control strategy for the standard n-trailer vehicle," in *IEEE Intelligent Vehicles Symposium (IV)*, Baden-Baden, Germany, Jun. 2011.

[9] I. Masar and R. Gabler, "An integrated environment for the modeling, simulation, and rapid design of control algorithms for mobile robots," Sep. 2005. [Online]. Available: http://www.mathworks.com/company/newsletters/digest/2005/sept/mobile_robots.html
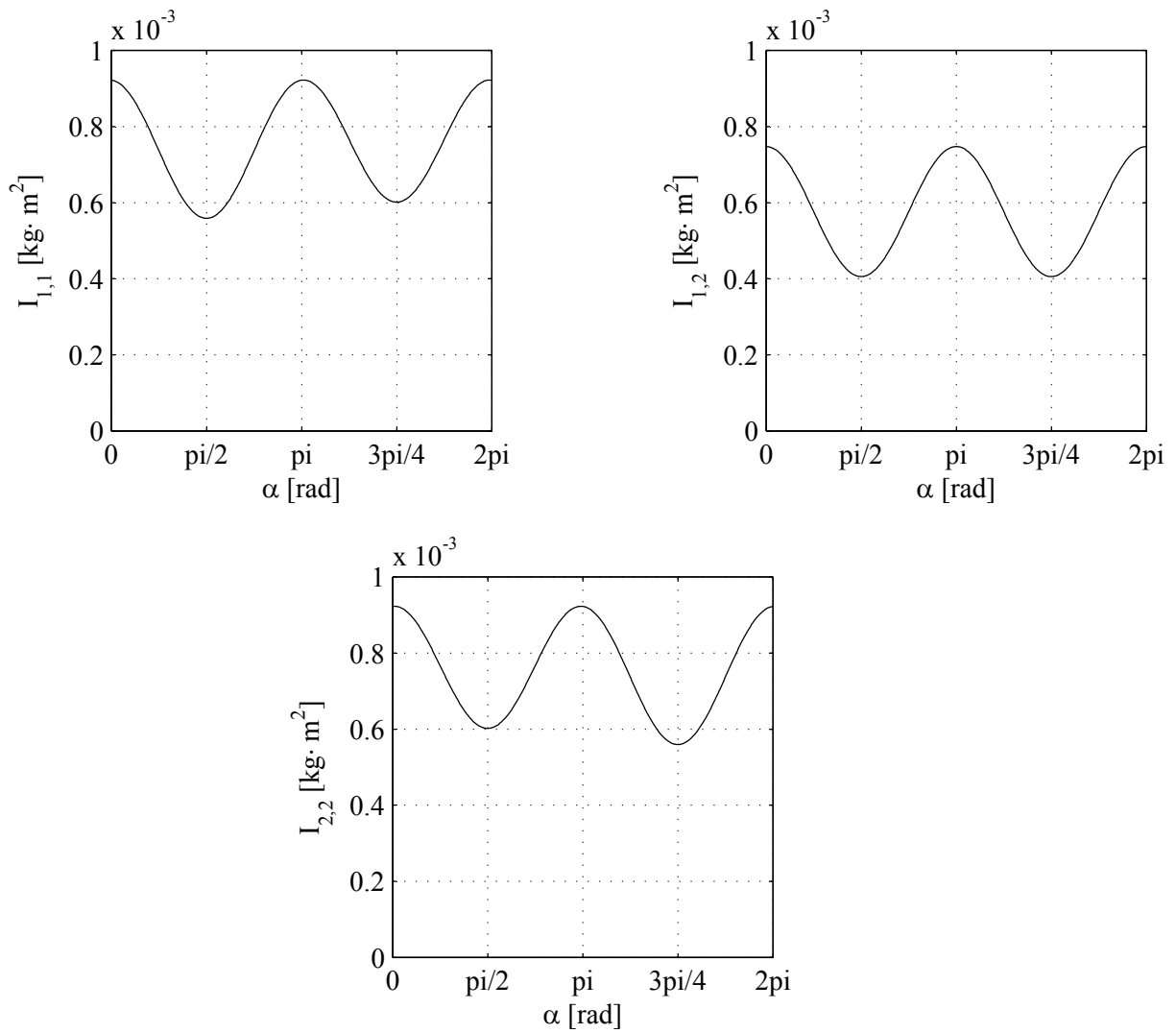
A   Generalized Inertia Matrix

Figure 26: The entries of the generalized inertia matrix $\mathbf{I}(\alpha)$.

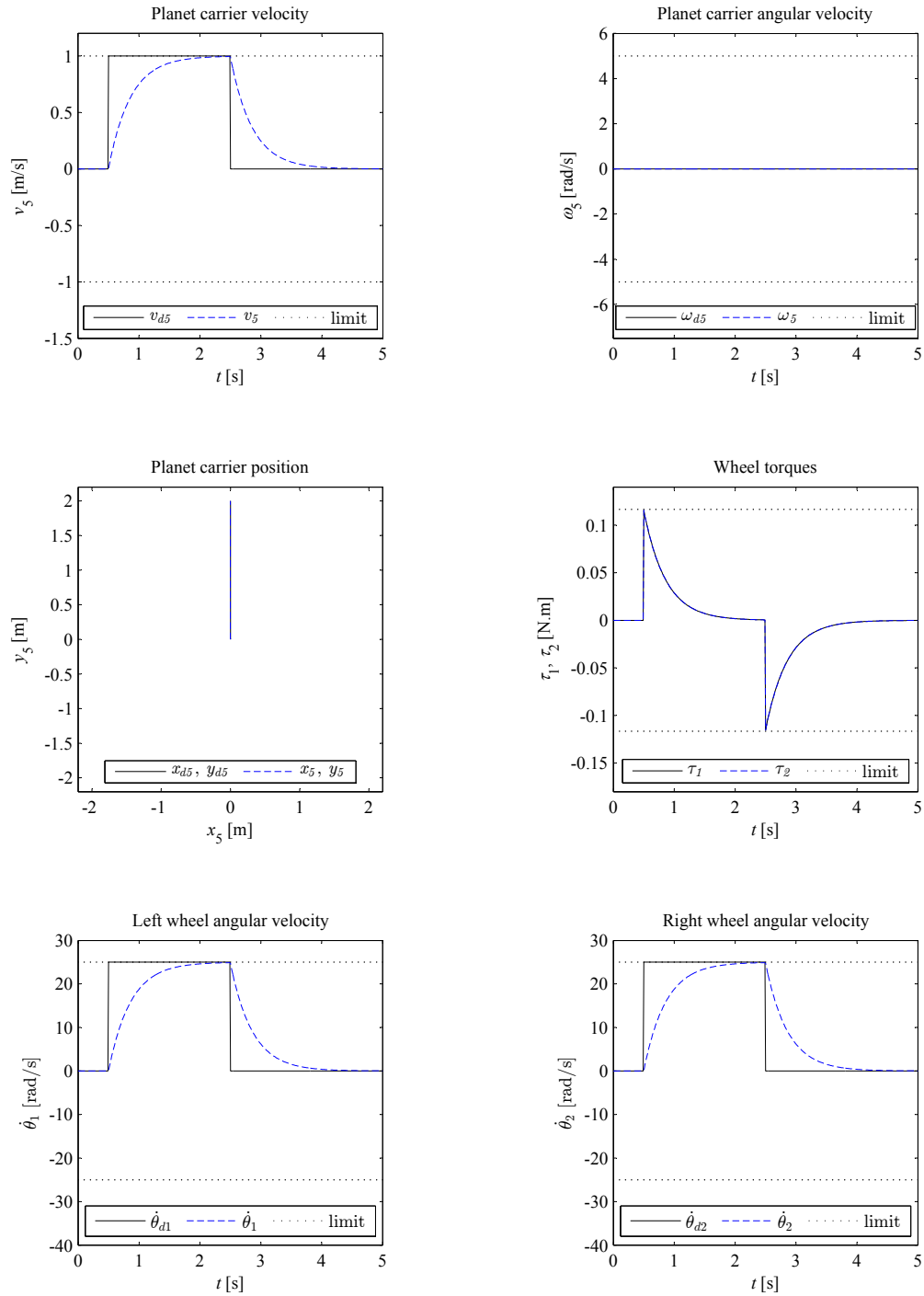# B   Simulation Results

B.1   Step-input

Figure 27: Straight trajectory step-input; desired and actual variables; $\rho = 2.78$ [1/s]; trajectory amplitude = 2.0 m; maximum velocity = 1.0 m/s.
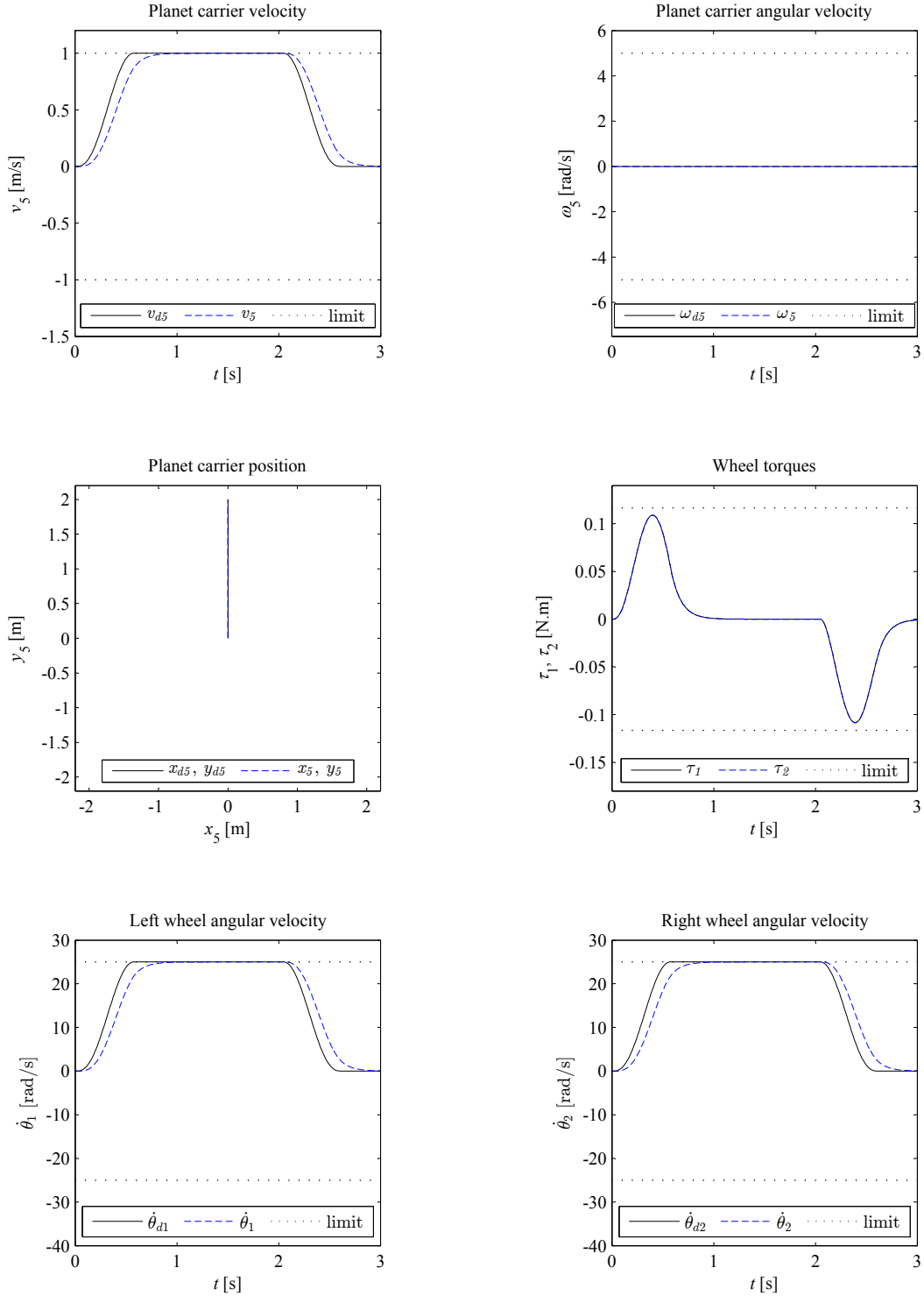
B.2 Straight trajectory

Figure 28: Straight trajectory; desired and actual variables; $\rho = 10.0$ [1/s]; trajectory amplitude = 2.0 m; maximum velocity = 1.0 m/s; maximum acceleration = 3.0 m/s².
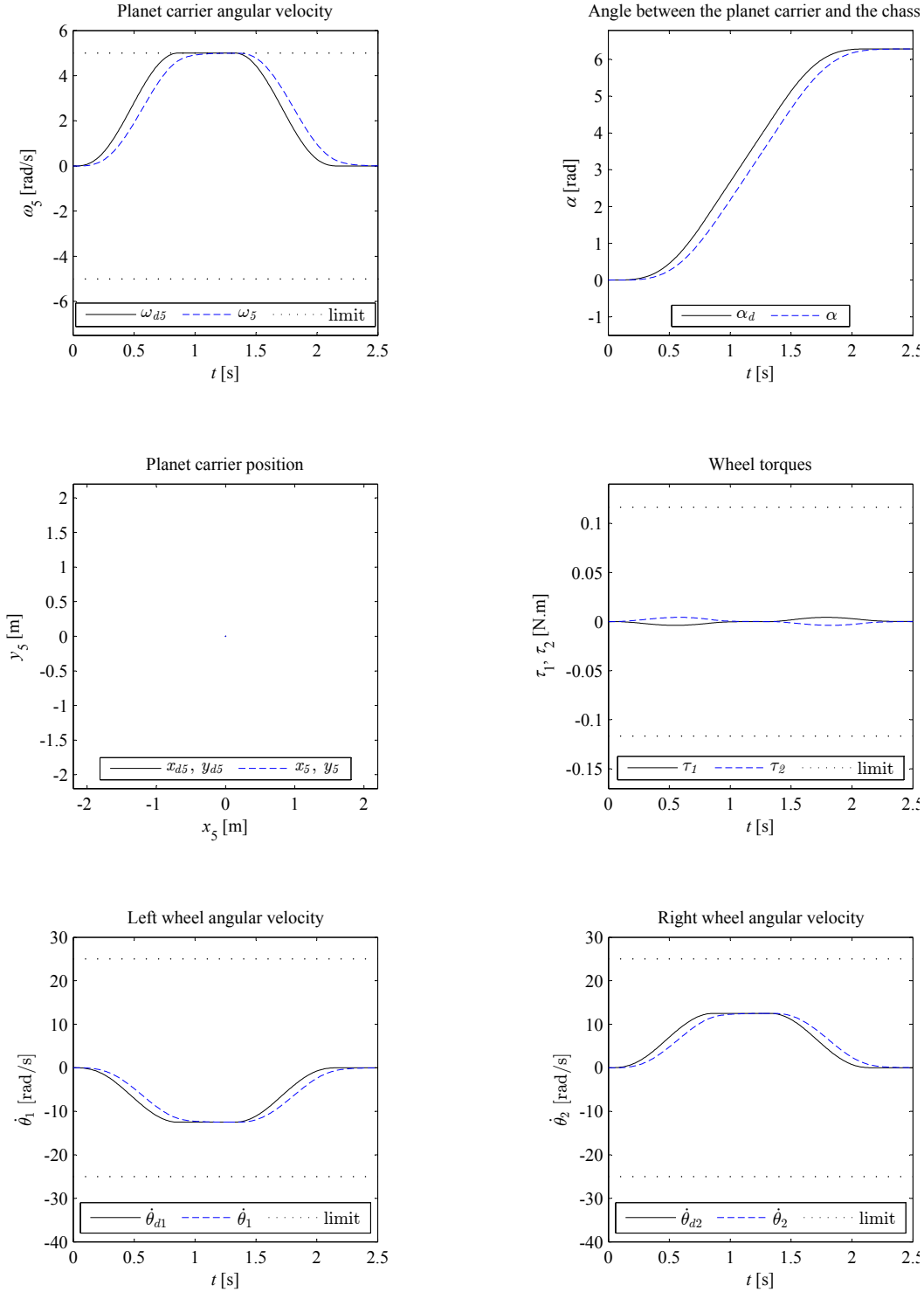
B.3 Rotation of the planet-carrier trajectory

Figure 29: Rotation of the planet-carrier trajectory; $\rho = 10.0$ [1/s]; trajectory amplitude $= 2\pi$ rad; maximum angular velocity $= 5.0$ rad/s; maximum angular acceleration $= 10.0$ rad/s^2.
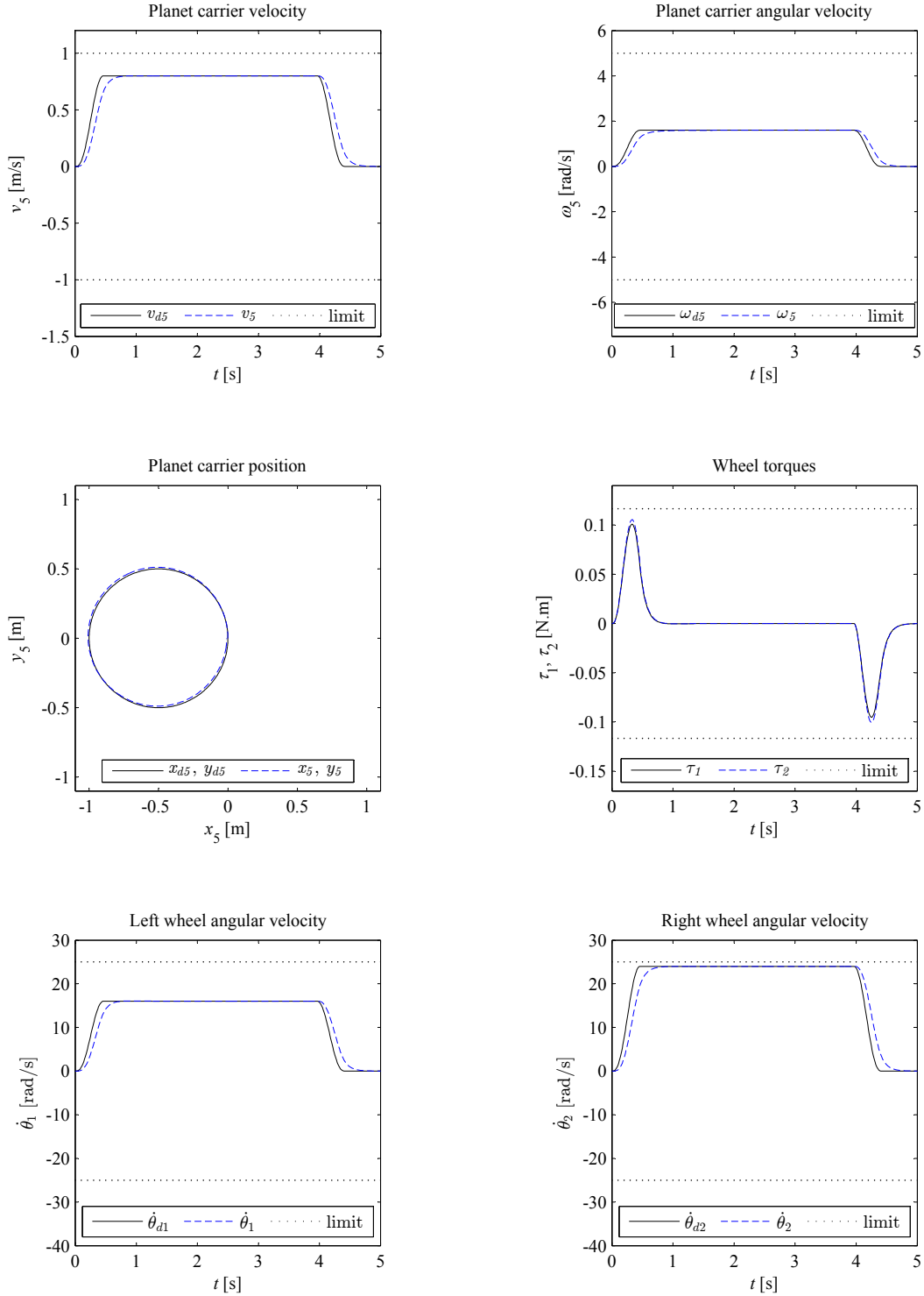
B.4 Circle trajectory

Figure 30: Circle trajectory; $\rho = 10.0$ [1/s]; radius $= 0.5$ m; angle $= 2\pi$ rad; maximum velocity $= 0.8$ m/s; maximum acceleration $= 3.0$ m/s^2.
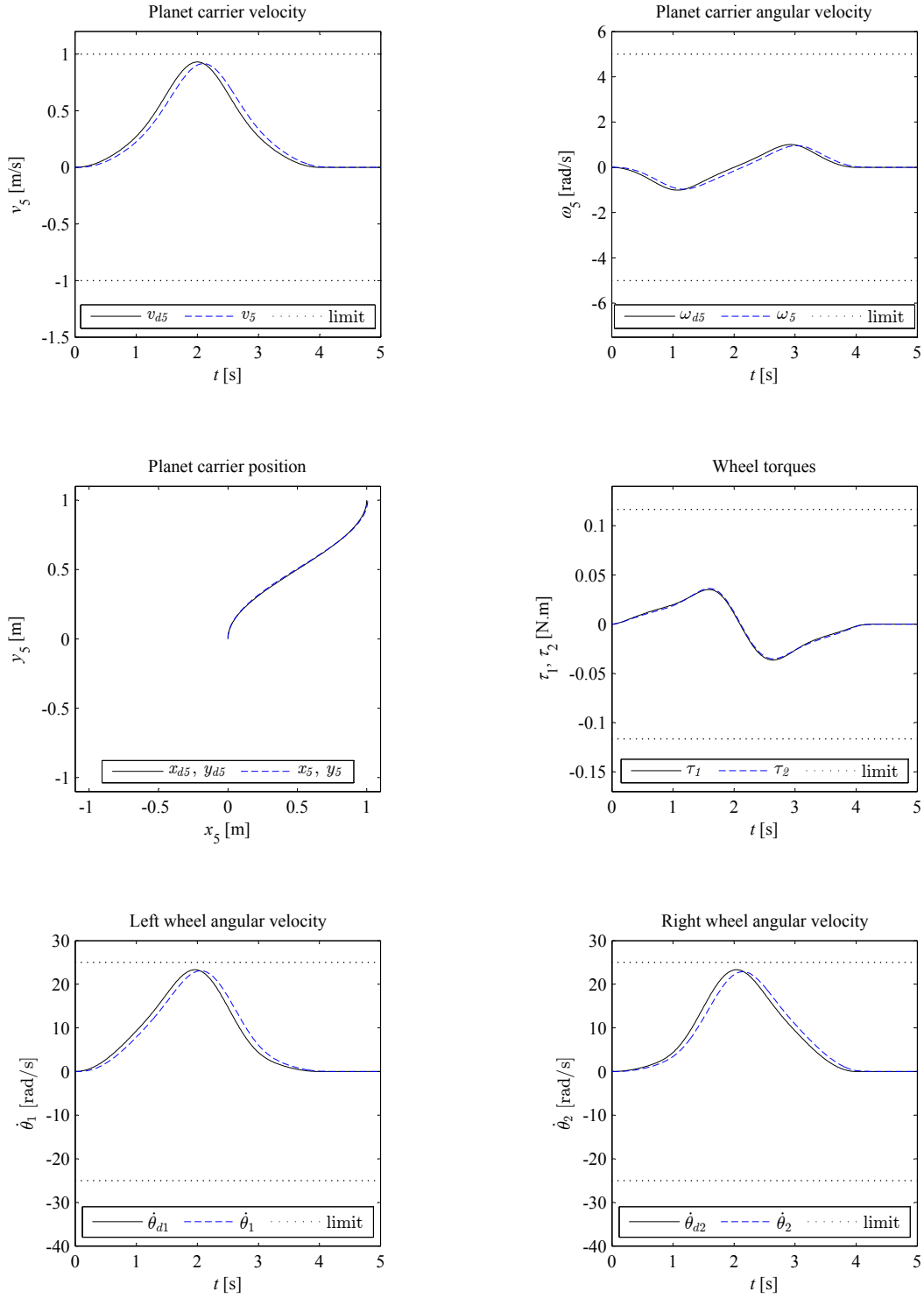
B.5   Parking trajectory

Figure 31: Parking trajectory; $\rho = 10.0$ [1/s]; task time = 4.0 s; $\Delta x = 1.0$ m; $\Delta y = 1.0$ m.